NATIONAL ADVISORY COMMITTEE FOR AERONAUTICS

TECHNICAL NOTE 3988

EXPERIMENTAL AND CALCULATED HISTORIES OF VAPORIZING FUEL DROPS

By R. J. Priem, G. L. Borman, M. M. El Wakil,
O. A. Uyehara, and P. S. Myers

The University of Wisconsin

Washington
August 1957

NATIONAL ADVISORY COMMITTEE FOR AERONAUTIC

TECHNICAL NOTE 3988

EXPERIMENTAL AND CALCULATED HISTORIES OF VAPORIZING FUEL DROPS

By R. J. Priem, G. L. Borman, M. M. El Wakil,
O. A. Uyehara, and P. S. Myers

SUMMARY

The present report contains the results of an experimental and theoretical investigation of the vaporization of fuel droplets in heated air under atmospheric pressure.

First, an experimental investigation of the temperature and mass histories of single droplets was made, with emphasis on small drops down to 500 microns.

Second, a comparison of experimental histories with calculated temperature and mass histories was made. In connection with the calculated histories, the equations of change and the associated boundary conditions are given in reduced form along with the various dimensionless parameters that would appear in a solution of these equations.

Third, the time taken by a droplet vaporizing in high-temperature air to form a mixture of fuel vapor and air of combustible strength in the film of the droplet and at the self-ignition temperature is calculated. The concept of physical ignition delay of single droplets is thus presented. In addition, the vaporization of fuel droplets in a spray under conditions where there exists an influence of one droplet on another is theoretically investigated.

The experimental and calculated results can be summarized as follows:

(1) An appreciable portion of the drop may be vaporized during the "heating-up" period; at high air temperatures as much as 50 percent or more of the mass may be vaporized during this period.

(2) Calculated and experimental times to reach the same percent mass vaporized differed by 20 percent on an average with the computed values usually smaller.

(3) For 500-micron drops, computations including the heating-up period gave better agreement with experimental results than did computations neglecting the heating-up period or assuming "peeling," that is,

zero thermal conductivity of the liquid. This is especially true for low-volatility fuels.

(4) The computed physical ignition delay of single droplets increases rapidly with decreased fuel volatility and decreased air temperature and is relatively insensitive to variations in total pressure.

(5) If there is interaction between the vaporizing drops in a spray, cooling of the air results, approaching, as a limit, the adiabatic equilibrium temperature. The higher the concentration and volatility of the fuel, the lower the adiabatic equilibrium temperature.

INTRODUCTION

Fuel which is injected into a combustion chamber by a nozzle leaves the nozzle orifice as sheets or ligaments which eventually break down into drops of varying sizes. As soon as these drops are formed they start to vaporize because of the increase of surface-to-volume ratio. As the drop vaporizes it simultaneously heats up until its temperature approaches asymptotically a constant temperature which is determined by the environmental conditions. Previous investigations of fuel ignition are discussed in references 1 to 16.

A detailed theoretical study of the unsteady-state portion of the total vaporization time for single droplets was performed in a previous investigation (ref. 1). From this study it was estimated that the larger drops emanating from the injector of a jet engine reach the combustion zone while still in the unsteady-state or heating-up period. After the importance of the unsteady state had been verified theoretically a combined theoretical and experimental investigation was undertaken to determine if the unsteady-state period was important (ref. 2). This combined investigation served to check the accuracy of the theoretical calculations.

The combined theoretical and experimental investigation showed that the theory used for the calculations produced histories which gave reasonable agreement with the experimental histories. The range of conditions covered by this first experimental investigation was limited to drop sizes in the neighborhood of 2,000-micron initial diameter and to a maximum air temperature of 1,080° R. In order to bring the experimental conditions closer to actual jet conditions the investigation was extended to smaller drop sizes, higher air temperatures, and different fuels. The results of this extended investigation are reported herein.

In addition to the extension of the range of conditions covered experimentally, comparisons were made with calculated histories to

determine and to illustrate the agreement between theoretical and experimental results. By plotting the comparisons against various parameters the trends of the theoretical accuracy are determined, thereby indicating the error that would be obtained by extrapolating the theoretical technique to conditions other than those covered in this investigation.

In order better to orient the above study to actual spray conditions some thought was given to the possible range of conditions found within the spray. Under spray conditions the assumption of no influence of one drop upon another may not be entirely valid. Two extreme cases may be encountered. The first of these is the case of the free drop; the other is the condition known as adiabatic equilibrium. In the case of adiabatic equilibrium the droplets cool the surrounding air, a condition that may be possible in the initial core of the spray. Actual spray conditions elsewhere probably fall somewhere between these extreme conditions.

Besides the problem of the effect of one drop upon another, there is the added problem that under most actual spray conditions the air temperature is high enough to cause self-ignition of the drops before they are completely vaporized. With the assumption of no influence of one drop upon another, a theory was developed which predicts the effect of various parameters upon the time required to form a combustible mixture. This time is defined as the physical-ignition-delay period.

The present investigation was conducted at the University of Wisconsin under the sponsorship and with the financial assistance of the National Advisory Committee for Aeronautics.

EXPERIMENTAL APPARATUS AND TECHNIQUES

The experimental temperature-time curves were obtained by hanging a drop of fuel on the junction of a thermocouple which was connected to a high-speed recorder. A stream of hot air was suddenly blown past the stationary drop (fig. 1). The velocity of the air was measured by a velometer. The radius-time curves were obtained by photographing the drop with a movie camera (fig. 2). The mass-time curves were then obtained by calculating the mass from the measured radii and the known densities at the measured temperatures.

To obtain the small drops discussed in this investigation it was necessary to make extremely small thermocouples. This proved to be a very difficult task. A thermocouple made of low-thermal-conductivity wire with a ratio of initial drop diameter to wire diameter of 20 to 1 or greater was used to minimize the conductive heat transfer. The accuracy of the temperature measurements as determined by the variation in the steady-state temperature was $\pm 4^{\circ}$.

The problem of placing a drop on the thermocouple limited the investigation to drops having an initial diameter of approximately 500 microns or more. With smaller drops there was insufficient time to transfer the drop to the thermocouple because it either evaporated completely on the wire or was too large to hang on the thermocouple.

The extremely short lifetimes of the small drops necessitated the use of a high-speed, direct-recording oscillograph. The instrument used has a response of 0.01 second for full-scale deflection and a maximum chart speed of 10 inches per second. Droplet histories with a total lifetime of 0.1 second could be recorded with this instrument.

The air heater (fig. 1) consists of tubular electric heaters with a maximum permissible sheath temperature of 2,060° R. The heat losses in the calming section were reduced by placing this section inside the heater. This location also reduced the temperature fluctuations in the test-section airstream. A maximum air temperature of 1,440° R with air flows up to 6 pounds per hour was obtained with this design.

The optical system for viewing and photographing the drops is shown in figure 2. The light source used in previous investigations was replaced by a Pointolite lamp which provided a greater intensity of illumination. A half-silvered mirror was used to provide two images. One image was photographed with the 16-millimeter movie camera and the other image was projected on a ground glass for visual observation. The magnification of the optical system was increased to 50 for studying small drops. The photographic system was calibrated by introducing a wire of known diameter at the location of the drop. The error for the 500-micron drops was estimated to be ±3 percent for the initial radius measurements and 5 percent for the final diameter.

EXPERIMENTAL RESULTS

More than 300 experimental histories have been obtained and studied. These histories covered 10 paraffin hydrocarbons ranging in volatility from n-hexane to n-octadecane. The air temperature was varied between 680° and 1,430° R; the air velocity, between 27 and 228 inches per second; and the initial drop diameter, between 490 and 2,180 microns. Drop histories were followed to a minimum drop size of 150 microns, that is, a size slightly greater than the bead size of the thermocouple.

In order to illustrate the type of information obtained figure 3 is presented. This figure gives liquid temperature, mass, and radius histories for small drops of different fuels. Figure 3(a) presents data taken with a low air temperature. Figure 3(b) presents data taken with a high air temperature.

The radius curves for high-molecular-weight fuels first increase and then decrease while the curves for low-molecular-weight fuels decrease immediately because the high-molecular-weight fuels initially expand thermally while not losing much mass by vaporization. It will also be noted in figure 3 that there was a variation in initial liquid temperature with fuel volatility. In general, no correction was made for this difference in initial liquid temperature.

Because of the large number of histories obtained it was decided to present the effect of the parameters studied, that is, air temperature, drop size, and fuel volatility, by cross plots of results. The points chosen for cross-plotting were the times required to reach the steady state and to vaporize 20, 50, and 80 percent of the original mass of the drop. The time to reach the steady state (i.e., the unsteady state) is the time required for the drop to reach its wet-bulb temperature.

Figure 4 presents cross plots for the parameter of air temperature against vaporization time for the fuels n-hexane, n-decane, and n-hexadecane. The data show that the time to reach the steady state decreases with higher air temperature and fuel volatility. The time required to reach the steady state also tends to approach a constant value asymptotically; this trend is more evident for the fuels with higher volatility.

Figure 5 presents cross plots for the parameter of fuel volatility as expressed by the normal boiling point at air temperatures of 900° and 1,430° R. The data show that all of the parameters plotted are less affected by fuel volatility at higher air temperatures. The trend is accentuated because the same initial liquid temperatures were not obtained for all fuels.

Cross plots of the parameter of initial drop size are presented in figure 6 for the fuels n-hexane, n-decane, and n-hexadecane. While it is not clearly evident in figure 6, other data show more clearly that, within the experimental accuracy, the time required for 20-, 50-, and 80-percent mass transfer and the unsteady-state time plot as straight lines in this figure. The slope of these lines (neglecting the unsteady-state time) was theoretically determined (ref. 2) as 2.0 for high air velocities and 1.5 for still air. Inasmuch as the slopes of the lines of 20-, 50-, and 80-percent mass transfer are all less than 1.5 it would appear that the effect of the unsteady-state time was to decrease the dependency on drop size. While not shown here, data similar to those in figure 6 but for lower air temperatures show a slightly greater dependency on initial drop diameter.

It can also be seen by the change in the location of the unsteady-state line with fuel volatility (see figs. 6(a) and 6(c)) that, with a heavy fuel, appreciably more mass is transferred during the unsteady state.

The steady-state temperature of a particular fuel was dependent on only the air temperature for the range of conditions covered, as illustrated in figure 7. The shaded area for each fuel represents the variation in the experimental data. The effect of size or velocity on the steady-state temperature was less than the experimental accuracy.

The times required to reach the steady-state temperature and various percents of the mass are enlightening and show the importance of the effect of various parameters on the vaporization period, but they do not indicate the relative importance of the heating-up period. Consequently, the percent of the mass that had been vaporized at the end of the heating-up period was plotted as a function of the air temperature (fig. 8). The shaded area represents the extremes of the variations obtained. All the experimental points fell within this area irrespective of fuel, size, velocity, and initial temperature; therefore, any effect of these variables on the percent of the mass transferred at the end of the heating-up period was less than the experimental accuracy. Figure 8 shows that at high air temperatures 50 percent or more of the vaporization process occurs during the unsteady-state period.

COMPARISON OF EXPERIMENTAL AND CALCULATED RESULTS

Histories obtained under the condition which gave the minimum deviation between experimental and calculated histories are given in figure 9(a), while histories showing the maximum deviation are given in figure 9(b). The histories for the large n-hexadecane droplet vaporizing in an airstream of 1,230° R (fig. 9(a)) show excellent agreement between experiment and theory. The variation between experiment and theory for maximum deviations (fig. 9(b)) is within the experimental accuracy except for the temperature histories where the greatest deviation was 15° at the "knee" of the theoretical curve.

The agreement between calculated and experimental steady-state temperatures is shown in figure 10 for three of the fuels studied. The difference between the two results is less than the experimental variation, which was estimated to be ±4°.

A comparison of the time required for 20-, 50-, and 80-percent mass transfer as obtained experimentally and as calculated is shown in figure 11. The shaded areas represent the regions in which all the points fell. The experimental accuracy was approximately ±10 percent. Any variation with air temperature or velocity was smaller than the experimental accuracy. The data indicate that at large drop sizes the experimental vaporization time was slightly less than that calculated, while for small drops the experimental time was approximately 20 percent greater than that calculated.

For comparison purposes calculations were performed considering the drop to be at the steady-state temperature throughout its lifetime. The solid lines of figures 11(a), 11(b), and 11(c) show the ratio of experimental to calculated times for 20-, 50-, and 80-percent mass transfer, respectively. For high-volatility fuels (n-hexane), almost the same agreement is obtained with or without consideration of the unsteady-state. For low-volatility fuels (n-hexadecane), a considerable error occurs when the heating-up period is neglected. These figures also show that the error in not considering the unsteady-state period increases rapidly as the drop size is reduced.

The effect of fuel volatility on the ratio of experimental to calculated time required to vaporize a fixed percentage of mass is better shown in figure 12, where the ratios of experimental to calculated vaporization times are plotted for an initial drop size of 500 microns. In figure 12(a), the three lower lines indicate the small variation obtained between the experiment and the calculation when the unsteady-state period is considered in the calculation. This figure shows a large variation with fuel volatility and clearly indicates the need for considering the unsteady-state vaporization period for low-volatility fuels.

A comparison of the time required to reach the steady state as determined by experiment and by calculation is given in figure 13 as a function of the normal boiling temperature of each fuel. The solid vertical lines represent the variation in the ratio of experimental time to calculated time. The figures clearly indicate that for high-volatility fuels the theory is in considerable error. For heavy fuels the agreement is very good, as was indicated in the sample history given in figure 9(a).

There is yet another technique for calculating vaporization times. This technique, commonly known as peeling, assumes that none of the heat arriving at the liquid surface goes to heat up the liquid drop; that is, there is zero liquid thermal conductivity. Therefore, the heat reaching the liquid surface just equals the heat needed to heat the vaporizing mass to the vaporizing temperature and to vaporize it. This vaporizing or surface temperature is lower than the steady-state temperature obtained experimentally.

Figure 12(b) shows the comparison of experimental results with calculations based on the peeling technique. This calculation technique produced better agreement than the one considering no unsteady state as given in figure 12(a). However, when using this calculation technique, the time for 20-percent vaporization is still very sensitive to fuel volatility, and for low-volatility fuels the error is quite large.

It should be remembered that in all the previous comparisons the air velocity was held constant during the lifetime of the drop. Similar comparisons would be found, however, if variable air velocities were considered.

DROPLET VAPORIZATION CALCULATIONS UNDER CONDITIONS FOUND IN SPRAYS

Vaporization conditions encountered in actual fuel sprays may be somewhat different from the conditions experimentally studied in this report. Reference 1 gave a calculation technique that may be used to include the variable droplet velocity as predicted by the drag coefficients and flow theory. Other considerations may be needed, however, in order to understand combustion in a spray better. Some thought was given to two of these considerations and the resulting theory was used to predict the possible effect of various parameters briefly.

The first situation considered is a drop injected into an atmosphere hot enough to cause self-ignition where there is no influence of one drop on another. The second situation considered was the cooling of the air by the vaporizing drops. The results of computations for drops vaporizing under these conditions will be presented below. The symbol list is given in appendix A and the theory and equations used to obtain these results are given in appendixes B and C. This theory was originally applied to Diesel engines and more extensive data and comparisons are given in reference 3.

Speaking of the first situation, as a droplet vaporizes in a high-temperature atmosphere a layer of fuel-air mixture builds up around the drop. The fuel-vapor-air mixture in the film varies in composition along radial lines from the drop, with the richest mixture being next to the droplet surface. The temperature in the film increases from the liquid temperature to the air temperature. As the droplet heats up, its vapor pressure increases until a combustible mixture is first found at the liquid surface. As the drop is heated to yet higher temperatures, this mixture moves away from the drop into a region of higher temperature.

When the steady-state liquid temperature is reached the vapor film will be fixed in both its partial pressure and temperature distribution. It can therefore be seen that if a combustible mixture (say stoichiometric) is to be formed around the drop at the self-ignition temperature it must occur before or at the steady state with the beginning of the steady state as the limiting time.

The time necessary to form a chemically correct mixture at the self-ignition temperature has been defined as the physical-ignition-delay period. It is supposed that any further ignition delay is due to chemical factors; that is, it will be chemical ignition delay.

The effect of air temperature upon the computed physical ignition delay of a drop of n-decane is shown in figure 14. The ignition delay

shows a sharp decrease with increasing air temperatures with a leveling off at higher air temperatures. The physical ignition delay goes to infinity at low temperatures, indicating that the combustible mixture, as previously defined, cannot form at its self-ignition temperature.

The results of computations (not presented here) when the total pressure was increased from 1/2 to 5 atmospheres gave only a small increase in physical ignition delay, indicating that the physical ignition delay is comparatively insensitive to variations in total pressure.

The higher volatility fuels form a stoichiometric mixture more rapidly (as shown in fig. 15) despite their lower molecular weight and the resulting necessity of a higher vapor pressure to form a stoichiometric mixture. It should be noted that heavier fuels reach a higher liquid temperature before a combustible mixture is formed and consequently they may experience cracking in the liquid phase before the combustible mixture is formed. This fact may be important in smoke and deposit problems.

The second situation is concerned with adiabatic equilibrium within a spray. The work previously reported in this paper assumed that a large excess of air always surrounded the vaporizing drop and that at no time did the vaporization process affect the temperature or composition of the air surrounding the drop except in the film. This assumption seems plausible in sprays where there is considerable distance between fuel droplets and where the fuel-air ratio is low. If, however, the core of the spray is considered it seems conceivable that the vaporization process may cool the surrounding air appreciably and that the fuel vapor in the atmosphere may reduce the driving force for mass transfer. The equations applicable under this assumption are given in appendix D. Briefly, it is assumed that there is no net heat or mass transfer to or from the section under consideration and that the air and fuel vapor external to the drop and its immediate film are uniform at any time.

Figures 16 and 17 show the results of calculations made using the theory of appendix D. Figure 16 is a plot of air-fuel-mixture temperature versus overall fuel-air ratio. This is a thermodynamic calculation and thus is not concerned with the amount of time necessary to reach this end condition. Figure 16 shows that a considerable drop in temperature may occur even for low fuel-air ratios. Fuel-air ratios as high or higher than stoichiometric (approximately 0.067) may occur in the primary zone and thus it seemed desirable to perform calculations which would give some indication of the time required to approach adiabatic equilibrium.

Figure 17(a) shows histories for drops of n-heptane vaporizing with fuel-air ratios of zero, 0.067, and 1.0. The temperature of the air and vapor drops rapidly while the mass and liquid temperature histories are affected only slightly as compared with those of pure air when a fuel-air

ratio of 0.067 is considered. The percent mass vaporized at any time decreases rapidly as the fuel-air ratio is increased. Figure 17(b) shows similar histories for n-hexadecane with similar conclusions.

The above conclusions and results were based solely on the theory presented in appendixes C and D. No direct experimental evidence was available for comparison with the theoretical predictions.

DISCUSSION OF RESULTS

The results of this investigation of the experimental and calculated temperature and mass histories of vaporizing fuel drops have shown that the unsteady-state vaporization period is important in the vaporization of low-volatility fuels of all size drops. For high-volatility fuels, such as n-hexane, where only the time for complete vaporization is of interest, there is less error in neglecting the heating-up period.

The calculation techniques described in reference 1 gave reasonably accurate histories of the percent mass transferred from the drop. The discrepancy between calculated and experimental histories for large drops and high-molecular-weight fuels is within the experimental accuracy, but the discrepancy increases with decreasing drop size and fuels with lower molecular weights to a maximum of 20 percent for n-hexane drops of 500-micron initial diameter. This indicates that the use of the calculation technique for very small drops might introduce a considerable error. The inclusion of the heating-up period in the calculations gives a significant improvement over other techniques for small drops.

The increase in error with decreasing drop size is believed to be due to the omission of the $P_A^*(t)$ term derived in appendix B. As the drop size decreases, the vaporization time also decreases, thereby producing a larger rate of change of pressure in $P_A^*(t)$. The $P_A^*(t)$ term would therefore increase with decreasing size and likewise the error introduced by neglecting it would increase.

Although the mass histories give reasonably good agreement the temperature histories obtained with the calculation technique described in reference 1 do not fully coincide with the experimental histories for both small drops and low-molecular-weight fuels as shown by figure 9. The discrepancy with drop size is believed to be due to the omission of the $\Delta T_L(t)$ term (appendix B), which would increase with decreasing drop size. The discrepancy with fuel volatility could result from the omission of the dimensionless term M_a/M_f, where M_a is the mass of the air and M_f is the mass of the fuel vapor.

If, because of their complexity, it is not feasible to perform the calculations including the unsteady state, it is suggested that calculations based on peeling be employed rather than calculations which consider the drop to be at the steady-state temperature throughout its lifetime. For example, the error in the vaporization time for 50- and 80-percent vaporization of a small drop of n-octadecane when using the steady-state calculation is 160 and 100 percent, respectively (fig. 12(a)), while if the peeling calculation is used the error is reduced to 50 and 10 percent, respectively (fig. 12(b)). The error in the 20-percent-vaporization time is not significantly decreased by use of the peeling calculation.

The theoretical work done on physical ignition delay indicates that this phenomenon may be of importance in cases where the fuel droplets are not completely vaporized before reaching a high-temperature zone. The theory again points out the importance of the unsteady-state portion of the histories. Drops injected in the reaction zone itself may exhibit behavior different from that indicated by the theory. Clearly a better understanding of chemical and physical delay is necessary to predict total ignition delay accurately.

Adiabatic equilibrium conditions may exist in the very core of a spray and a short distance from the nozzle, but the calculations performed here show the effects of these conditions to be negligible unless the fuel-air ratio is above stoichiometric. This analysis gives another indication that single-droplet calculations may be applied to the major portion of the spray without great error.

The University of Wisconsin,
Madison, Wisc., July 6, 1955.

APPENDIX A

SYMBOLS

A_o	surface area of liquid drop, sq in.
B_o	thickness of air-vapor film surrounding drop, in.
$C_1 = K_m P_{fL} k_{Nu} / P_T$	
$C_2 = Q_v - wc_{pf} T_L$	
$C_3 = wc_{pf}$	
c_p	specific heat at constant pressure, Btu/(lb)(°F)
D	diffusion coefficient of air-vapor system, sq in./sec
d_{v_f}	molar rate of diffusion of fuel vapor at liquid surface, mole/(sq in.)(sec)
d_{v_i}	diffusion velocity of component i with respect to a plane moving at mass average velocity, in./sec
f	molar mass flux vector with respect to liquid surface, mole/(sq in.)(sec)
g	acceleration due to gravity, in./sec^2
H_{Nu}	Nusselt number for heat transfer, dimensionless
J	mechanical equivalent of heat, (in.)(lb)/Btu
J_i	mass flux vector of component i with respect to plane moving at mass-average velocity, lb/(sq in.)(sec)
K	thermal conductivity, Btu/(in.)(sec)(°F)
K_m	average thermal conductivity in air-vapor mixture, Btu/(in.)(sec)(°F)
k	coefficient of mass transfer, 1/sec

k_{Nu}	Nusselt number for mass transfer, dimensionless
L_o	scale factor for length, in.
M	mass, lb
M_{t_1}, M_{t_2}	mass of drop at beginning and end of increment of time, respectively, lb
m_i	molecular mass of component i, lb/mole
n	total number density, mole/cu in.
n_i	number density of component i, mole/cu in.
P	partial pressure, lb/sq in.
P_T	total pressure, lb/sq in.
Pr	Prandtl number, dimensionless
$P_A^*(t)$	change in fuel vapor pressure as a function of time
$P_{fLv}(\theta)$	vapor pressure gradient at liquid surface at zero time as function of θ, lb/cu in.
Q	total heat transfer from air to drop, Btu/sec
Q_L	heat received at drop surface, Btu/sec
Q_r	sensible heat received by drop, Btu/sec
Q_s	heat carried back with diffusing vapor in form of superheat, Btu/sec
Q_{v_0}	heat transfer rate at zero time, Btu/sec
Q_λ	heat of vaporization, Btu/sec
R	universal gas constant, (in.)(lb)/(mole)($^\circ$F)
Re	Reynolds number, dimensionless
r	radius at any point in film, in.
r_d	radius of drop, in.

Sc	Schmidt number, dimensionless
T	temperature in film at radius r, $^{\circ}R$
T_B	air temperature at film boundary, $^{\circ}R$
T_i	intermediate temperature (see appendix D), $^{\circ}R$
T_L	temperature of liquid drop, $^{\circ}R$
T_m	mean temperature in film, $^{\circ}R$
$\Delta T_L(t)$	change in liquid temperature as a function of time, $^{\circ}R$
$T_{Lv}(\theta)$	gradient of film temperature at liquid surface at zero time as a function of θ, $^{\circ}R/in.$
t	time, sec
t_n	any time increment
V	velocity, in./sec
V_r^*	reduced radial velocity, dimensionless
V_θ	angular velocity, radian/sec
W	molecular weight, lb/mole
$\overline{W}_a, \overline{W}_f$	weight of air and fuel, respectively, in atmosphere
w	mass vaporization rate, lb/sec
w_O	mass transfer rate at zero time, lb/sec
X	body forces
y	fuel-air ratio by weight
α	correction factor for mass transfer, dimensionless
$\alpha' = \left[P_T \middle/ \left(P_{fL} - P_{fB}\right)\right] \log_e \left[\left(P_T - P_{fB}\right) \middle/ \left(P_T - P_{fL}\right)\right]$	
β	dimensionless number, M_a/M_f

Γ	dimensionless number, $Q_{v_o} L_o / KA_o T_o$
Θ	dimensionless number, $P_o / (P_{fL} - P_{fB})$
ϑ	dimensionless number, $T_o / (T_B - T_L)$
η	pressure number, $\frac{\rho_o V_o^2}{g P_o}$
θ	angle
λ	heat of vaporization, Btu/lb
μ	viscosity, lb/(in.)(sec)
ρ	density, lb/cu in.
ρ_m	mass density of mixture, lb/cu in.
τ	reduced surface area, dimensionless
Φ	dissipation function, $1/sec^2$
ψ	dimensionless number, $L_o w_o c_{p_o} / K_o A_o$
χ	dimensionless number, P_2 / P_o
ω	total mass flow from drop
∇	del operator, $\tilde{i}_1 \frac{\partial}{\partial x_1} + \tilde{i}_2 \frac{\partial}{\partial x_2} + \tilde{i}_3 \frac{\partial}{\partial x_3}$
$\partial^*/\partial r$	reduced radial gradient, dimensionless
$\partial^*/\partial \theta$	reduced angular gradient, dimensionless
$()^*$	reduced variable, dimensionless

Subscripts:

A	component A
a	air
B	at film boundary

f	fuel vapor
L	liquid or at liquid surface
o	scale factor
i	component i
1	component 1
2	component 2
T	total
v	rate or gradient
s	value with respect to space-fixed axis
0	at time zero

APPENDIX B

THEORY FOR DROP VAPORIZING IN HOT AIRSTREAM

The problem of a drop vaporizing in a hot airstream covers the problem of simultaneous transfer of heat and mass in a flow system. Such systems can be accurately described by the "equations of change" of fluid mechanics. These equations of change are the equation of continuity for each of the chemical species, the equation of motion, and the equation of energy balance. The various dimensional groups that should be correlated to form an experimental solution can be predicted from these equations when they are written in dimensionless form.

Mass Transfer

The transport of mass as described in reference 4 is dependent on (1) a gradient in the chemical potential, (2) a gradient in the total pressure, (3) a gradient in the temperature of the gas, and (4) transport due to external forces. The gradients in the total pressure and temperature are considered to be negligibly small in regard to both position and time in this presentation. The transport of mass per unit area because of a gradient in the chemical potential is determined from the following flux equation:

$$j_i = n_i m_i d_{v_i} \tag{B1}$$

For a two-component system, assuming an ideal gas and no pressure gradient in the vapor tangential to the liquid surface, this equation becomes for a spherical drop

$$f_1 = \frac{P_T}{P_2} \frac{D}{RT} \left(\frac{\partial P_1}{\partial r} \right)_{r=r_o} \tag{B2}$$

If the total pressure, partial pressure of component 2, D, R, and T are all constant over the entire surface, equation (B2) can be integrated over the entire surface to obtain the total mass flow from the drop or

$$\omega = \frac{P_T}{P_2} M_f \frac{DA_o}{RT} \int_S \left(\frac{\partial P_1}{\partial r} \right)_{r=r_o} d\tau \tag{B3}$$

Two arbitrarily chosen scale factors (indicated by a subscript o), the length L_o and pressure P_o, are now introduced. It is convenient to introduce the following transformed (reduced) variables (indicated by a superscript *) in terms of these scale factors:

$$P_i^* = P_i/P_o$$

$$r^* = r/L_o$$

Introducing the difference between the partial pressure of the fuel vapor at the liquid surface and that at infinity (or the film boundary),

$$\omega = A_o \frac{P_T}{P_2} \frac{M_f D}{RT} \left(\frac{P_{fL} - P_{fB}}{L_o} \right) \int_S \left(\frac{P_o}{P_{fL} - P_{fB}} \right) \left(\frac{\partial P_l^*}{\partial r^*} \right)_{r=r_o} d\tau \qquad (B4)$$

The pressure gradient $\partial P_l/\partial r^*$, the diffusion coefficient, and the temperature are evaluated at the liquid surface. The integral in equation (B4) is similar to the integral which Schlichting obtained for heat transfer (ref. 5). The integral in equation (B4) will be defined as the Nusselt number for mass transfer; that is,

$$k_{Nu} = \int_S \left[\frac{P_o}{P_{fL} - P_{fB}} \right] \left(\frac{\partial P_l^*}{\partial r^*} \right)_{r=r_o} d\tau \qquad (B5)$$

The functional form of this equation will be obtained later.

Heat Transfer

The transport of energy is dependent on (1) the temperature gradient, (2) the transport of thermal energy by the flux of the molecules, and (3) the reciprocal process to thermal diffusion known as the "Dufour effect." By neglecting the Dufour effect the heat transfer to a spherically symmetrical liquid drop was shown in reference 2 to be

$$Q_v = -KA_o \int_S \left(\frac{\partial T}{\partial r} \right)_{r=r_o} d\tau \qquad (B6)$$

When the scale factor T_o is used, $T^* = T/T_o$, and, introducing the difference in temperature at infinity (or the film boundary) and at the liquid surface,

$$Q_v = -KA_o\left(\frac{T_B - T_L}{L_o}\right)\int_S \left(\frac{T_o}{T_B - T_L}\right)\left(\frac{\partial T^*}{\partial r^*}\right)_{r=r_o} d\tau \qquad (B7)$$

It is understood that the temperature gradient $\partial T^*/\partial r^*$ and the thermal conductivity K are evaluated at the liquid surface. The integral in equation (B8) is similar to the integral which Schlichting (ref. 5) called the Nusselt number for heat transfer or

$$H_{Nu} = \int_S \left(\frac{T_o}{T_B - T_L}\right)\left(\frac{\partial T^*}{\partial r^*}\right)_{r=r_o} d\tau \qquad (B8)$$

The functional form of this equation is given in the next section.

Air-Vapor Film

The four equations of change needed to describe the film surrounding the liquid drop are: (1) Equation of continuity for component A, (2) equation of continuity for the mixture as a whole, (3) equation of motion, and (4) equation of energy balance. The equation of continuity for component A is given in reference 4 and the equations of continuity of the mixture, motion, and energy balance are found in reference 6. All the equations are applicable to turbulent or laminar flow.

Equation of continuity for a mixture.- The continuity equation for a mixture of compressible fluids is

$$\frac{D\rho_m}{Dt} + (\nabla \cdot \rho\tilde{V}) = 0 \qquad (B9)$$

where the operator D/Dt is the substantial derivative.

Equation of energy balance.- The energy-balance equation for a perfect gas is

$$\rho_m \frac{D(c_pT)}{Dt} = -\frac{1}{J}\frac{DP}{Dt} + (\nabla \cdot K\nabla T) + \frac{\mu}{gJ}\Phi \qquad (B10)$$

Equation of motion.- For a compressible fluid, the equation of motion is

$$\rho_m \frac{D\tilde{V}}{Dt} = -g\nabla P + \rho_m \tilde{X} + (\nabla \cdot \mu\nabla\tilde{V}) + \frac{1}{3}\nabla(\mu\nabla \cdot \tilde{V}) \tag{B11}$$

Equation of continuity for component A.- The continuity equation of component A for compressible fluids is

$$\frac{DP_i}{Dt} = -(\nabla \cdot \rho\tilde{V}) - (\nabla \cdot \tilde{J}_1) \tag{B12}$$

In addition to these differential equations, it is necessary to know the pressure and temperature dependence of the physical properties. These functions are denoted as follows:

$$\left.\begin{aligned} \rho &= \rho(P_A,T) \\ c_p &= c_p(P_A,T) \\ \mu &= \mu(P_A,T) \\ K &= K(P_A,T) \\ D &= D(P_A,T) \end{aligned}\right\} \tag{B13}$$

The following scale factors are also introduced: The length L_e, velocity V_o, density ρ_o, temperature T_o, pressure P_o, specific heat c_{p_o}, viscosity μ_o, thermal conductivity K_o, and diffusion coefficient D_o.

In the following discussion the properties c_p, μ, and K are assumed to be constant at some appropriate mean value. With this assumption it is convenient to pick the scale factors c_{p_o}, μ_o, and K_o identical to these mean values so that μ^*, K^*, and c_p^* as defined on the following page are unity. The following reduced variables are thus defined:

Radius	$r^* = r/L_o$
Radial velocity	$V_r^* = V_r/V_o$
Angular velocity	$V_\theta^* = V_\theta L_o/V_o$
Density	$\rho^* = \rho_n/\rho_o$
Time	$t^* = tV_o/L_o$
Pressure	$P_i^* = P_i/P_o$
Viscosity	$\mu^* = \mu/\mu_o \equiv 1$
Thermal conductivity	$K^* = K/K_o \equiv 1$
Specific heat	$c_p^* = c_p/c_{p_o} \equiv 1$
Temperature	$T^* = T/T_o$
Diffusion coefficient	$D^* = D/D_o$
Molecular gas constant	$\frac{R^*}{M^*} = \frac{R}{M}\frac{T_o g}{V_o^2}$
Radial derivative	$\frac{\partial^*}{\partial r} = L_o \frac{\partial}{\partial r}$

The four equations of change are then rewritten in spherical coordinates with the further simplifying assumption that the body forces X_s and the dissipation function Φ are negligible.

The equation of energy balance:

$$\rho^* \frac{\partial T^*}{\partial t^*} = \left(\frac{K_o}{c_{p_o} L_o \rho_o V_o}\right)\left[\frac{\partial^*}{\partial r}\left(r^* \frac{\partial T^*}{\partial r^*}\right) + \frac{1}{\sin\theta}\frac{\partial}{\partial\theta}\left(\sin\theta \frac{\partial T^*}{\partial\theta}\right)\right] \tag{B14}$$

The equation of continuity:

$$\frac{\partial^*}{\partial t^*}(\rho^*) + \frac{1}{(r^*)^2}\frac{\partial^*}{\partial r}\left[\rho^* V_r^* (r^*)^2\right] + \frac{1}{r^* \sin\theta}\frac{\partial}{\partial\theta}\left[(\sin\theta)\rho^* V_o^*\right] = 0 \tag{B15}$$

The equations of motion:

$$\rho^* \frac{\partial}{\partial t^*}(V_r^*) = \left(\frac{gP_o}{\rho_o V_o^2}\right)\frac{\partial P^*}{\partial r^*} + \left(\frac{\mu_o}{V_o L_o \rho_o}\right)\frac{1}{(r^*)^2}\left\{\frac{\partial^*}{\partial r}\left[(r^*)^2 \frac{\partial V_r^*}{\partial r^*}\right] + \frac{1}{\sin\theta}\frac{\partial}{\partial\theta}\left(\sin\theta \frac{\partial V_r^*}{\partial\theta}\right)\right\} + \left(\frac{\mu_o}{V_o L_o \rho_o}\right)\frac{1}{3r^*}\left\{\frac{\partial}{\partial r^*}\left[(r^*)^2 V_r^*\right] + \frac{\partial^2}{\partial r^*}\left[(r^*)^2 V_r^*\right]\right\} \tag{B16}$$

$$\rho^* \frac{\partial}{\partial t^*}(V_\theta^*) = \left(\frac{gP_o}{\rho_o V_o^2}\right)\frac{1}{r^*}\frac{\partial P^*}{\partial \theta} + \left(\frac{\mu_o}{V_o L_o \rho_o}\right)\frac{1}{(r^*)^2}\left\{\frac{1}{\sin\theta}\frac{\partial}{\partial\theta}\left(\sin\theta\,\frac{\partial V_\theta^*}{\partial\theta}\right) + \frac{\partial^*}{\partial r}\left[(r^*)^2\frac{\partial V_\theta^*}{\partial\theta}\right]\right\} + \left(\frac{\mu_o}{V_o L_o \rho_o}\right)\frac{1}{3r^*}\left[-\cot\theta\csc\theta\frac{\partial}{\partial\theta}\left(\sin\theta\,V_\theta^*\right) + \frac{1}{\sin\theta}\frac{\partial^2}{\partial\theta^2}\left(\sin\theta\,V_\theta^*\right) + \frac{\partial^2}{\partial\theta\,\partial r^*}(r^*)^2 V_\theta^*\right] \tag{B17}$$

The continuity equation for component A:

$$\frac{\partial^* P^*}{\partial t^*} = -\frac{1}{(r^*)^2}\frac{\partial^*}{\partial r}\left[\rho^*(r^*)^2 V_r^*\right] - \frac{1}{r^*\sin\theta}\frac{\partial}{\partial\theta}\left(\rho^*\sin\theta\,V_\theta^*\right) + \left(\frac{D_o}{V_o L_o}\right)\frac{1}{(r^*)^2}\frac{\partial^*}{\partial r}\left[\frac{(r^*)^2 M^*(P_T^*)^2}{T^* R^* P_2^*} D^* \frac{\partial^*(P_A^*/P_T^*)}{\partial r^*} + \frac{r^* M^*(P_T^*)^2}{T^* R^* P_2^*} D^* \frac{\partial^*(P_A^*/P_T^*)}{\partial\theta}\right] + \left(\frac{D_o}{V_o L_o}\right)\frac{1}{r^*\sin\theta}\frac{\partial}{\partial\theta}\left[\sin\theta\,\frac{M^*(P_T^*)^2 D^*}{T^* R^* P_2^*}\frac{\partial^* P_A^* P_T^*}{\partial r} + r^*\sin\theta\,\frac{M^* P_T^* D^*}{T^* R^* P_2^*}\frac{\partial^*(P_A^*/P_T^*)}{\partial\theta}\right] \tag{B18}$$

The four dimensionless parameters which appear above are related to well-known dimensionless numbers in the following ways:

$$\left(\frac{\mu_o}{L_o V_o P_o}\right) = \frac{1}{Re}$$

$$\left(\frac{D_o}{V_o L_o}\right) = \left(\frac{D_o P_o}{\mu_o}\right)\left(\frac{\mu_o}{L_o V_o P_o}\right) = \frac{1}{Sc}\frac{1}{Re}$$

$$\left(\frac{K_o}{c_{p_o} L_o \rho_o V_o}\right) = \left(\frac{K_o}{c_{p_o} \mu_o}\right)\left(\frac{\mu_o}{L_o V_o \rho_o}\right) = \frac{1}{Pr}\frac{1}{Re}$$

$$\left(\frac{gP_o}{\rho_o V_o^2}\right) = \frac{1}{\eta}$$

where

Re	Reynolds number
Sc	Schmidt number
Pr	Prandtl number
η	pressure number

Additional dimensionless parameters might appear when one assumes special forms for the temperature and pressure dependence of the physical properties of equations (B13). For example, the ratio of the molecular weights appears if an ideal gas is assumed.

In addition to the system of equations given above, the boundary conditions of the problem must be specified. The boundary conditions are as follows:

For pressure:

(a) $P_A^* = 0$ at $r = \infty$ for all times and angles

(b) $\frac{\partial^* P_A^*}{\partial r} = 0$ at $r = \infty$ for all times and angles

(c) $\frac{\partial P_A^*}{\partial \theta} = 0$ at $r = r_o$ for all times and angles

(d) $P_A^* = P_A^*(t)$ at $r = r_o$ for all angles

(e) $\frac{\partial^* P_A^*}{\partial r} = P_{fLv}(\theta)$ at $r = r_o$ at zero time

For temperature:

(f) $T^* = 1$ at $r = \infty$ for all times and angles

(g) $\frac{\partial^* T^*}{\partial r} = 0$ at $r = \infty$ for all times and angles

(h) $\frac{\partial T^*}{\partial \theta} = 0$ at $r = r_o$ for all times and angles

(i) $T^* = T^*(t)$ at $r = r_o$ for all angles

(j) $\frac{\partial^* T^*}{\partial r} = T_{Lv}(\theta)$ at $r = r_o$ at zero time

For radial velocity:

(k) $V_r^* = 1$ at $r = \infty$ for all times and $\theta = 0$

(l) $V_r^* = 1$ at $r = \infty$ for all times and $\theta = \pi$

(m) $V_r^* = 0$ at $r = r_o$ for all times and all angles

(n) $\frac{\partial^* V_r^*}{\partial r} = 0$ at $r = r_o$ for all times and all angles

(o) $V_r^* = 0$ at all radii and times and $\theta = \pi/2$

For angular velocity:

(p) $V_\theta^* = 1$ at $r = \infty$ for all times and $\theta = \pi/2$

(q) $V_\theta^* = 0$ at $r = r_o$ for all times and all angles

(r) $\frac{\partial^* V_\theta^*}{\partial r} = 0$ at $r = r_o$ for all times and all angles

(s) $V_\theta^* = 0$ at all radii and times and $\theta = 0$

(t) $V_\theta^* = 0$ at all radii and times and $\theta = \pi$

Conditions (k), (l), and (p) specify that the scale factor V_o will be taken equal to the free airstream velocity. Condition (f) specifies that the scale factor T_o will be equal to the airstream temperature.

With these boundary conditions and the dimensionless numbers obtained in equations (B14) to (B18), the temperature, partial pressure of component A, radial velocity, and angular velocity are all seen to be functions of:

(1) Reynolds number

(2) Prandtl number

(3) Schmidt number

(4) Pressure number

(5) Pressure gradient at the liquid surface at zero time

(6) Temperature gradient at the liquid surface at zero time

(7) Change in partial pressure of component A with time

(8) Change in temperature of the liquid surface with time

(9) Radius

(10) Angle

(11) Time

That is,

$$T^* = T\left(Re, Pr, Sc, \eta, p_A^*(t), T^*(t), P_{fLv}(\theta), T_{Lv}(\theta), r^*, \theta^*, t^*\right) \quad (B19)$$

$$P^* = P(Re, \ldots t^*) \quad (B20)$$

$$V_r^* = V_r(Re, \ldots t^*) \quad (B21)$$

$$V_\theta^* = V_\theta(Re, \ldots t^*) \quad (B22)$$

Since the gradients of the pressure and temperature at the liquid surface cannot be determined directly, it is convenient to transform these terms by use of equations (B4) and (B7):

$$w_O = A_O \frac{P_T}{P_2} \frac{M_f D}{RT} \frac{P_O}{L_O} \int_S \left(\frac{\partial P_1^*}{\partial r^*}\right)_{r=r_O} d\tau \quad (B23)$$

$$\frac{\partial P_a^*(\theta)}{\partial r^*} = f\left[\left(\frac{w_O R T L_O P_2}{A_O M_f P_T D P_O}\right)\theta^*\right] \quad (B24)$$

and

$$Q_{vO} = -KA_O \frac{T_O}{L_O} \int_S \left(\frac{\partial^* T^*}{\partial r^*}\right)_{r=r_O} d\tau \quad (B25)$$

$$\frac{\partial T^*(\theta)}{\partial r^*} = f(\Gamma\theta^*) \tag{B26}$$

where $\Gamma = Q_{v_0} L_o / KA_o T_o$, w_0 is the mass transfer rate at zero time, and Q_{v_0} is the heat transfer rate at zero time. The dimensionless parameter which appears in equation (B24) can be written

$$\left(\frac{w_0 RTL_o R_2}{A_o M_f D P_o P_T}\right) = \left(\frac{\mu_o}{D_o \rho_o}\right)\left(\frac{K_o}{c_{p_o}\mu_o}\right)\left(\frac{L_o w_0 c_{p_o}}{K_o A_o}\right)\left(\frac{RT_o\rho_o}{M_a P_T}\right)\left(\frac{M_a}{M_f}\right)\left(\frac{P_2}{P_o}\right) \tag{B27}$$

For a perfect gas $\frac{RT_o\rho_o}{M_a P_T} = 1$; therefore,

$$\left(\frac{w_0 RTL_o P_2}{A_o M_f D P_o P_T}\right) = Sc\ \frac{1}{Pr}\ \psi\beta\chi \tag{B28}$$

where

$$\beta = \left(\frac{M_a}{M_f}\right)$$

$$\psi = \left(\frac{L_o w_0 c_{p_o}}{K_o A_o}\right)$$

$$\chi = \left(\frac{P_2}{P_o}\right) = \left(\frac{P_T - P_{fL}}{P_o}\right)$$

In terms of these new dimensionless numbers, the functional forms of the temperature and partial pressure of component A become:

$$T^* = T\left(Re,\ Pr,\ Sc,\ \eta,\ P_A^*(t),\ T^*(t),\ \beta,\ \Gamma,\ \psi,\ \chi,\ r^*,\ \theta^*,\ t^*\right) \tag{B29}$$

$$P^* = P(Re,\ \ldots\ t^*) \tag{B30}$$

Introducing the notation

$$\vartheta = \left(\frac{T_o}{T_B - T_L}\right)$$

$$\Theta = \left(\frac{P_o}{P_{fL} - P_{fB}}\right)$$

the Nusselt numbers can be defined in the functional form as follows:

$$H_{Nu} = H\left(\Theta, Re, Pr, Sc, \eta, P_A^*(t), T^*(t), \beta, \psi, \chi, \Gamma\right) \qquad (B31)$$

$$k_{Nu} = k(\vartheta, Re, Pr, Sc, \eta, P_A^*(t), T^*(t), \beta, \psi, \chi, \Gamma) \qquad (B32)$$

It is seen, therefore, that the Nusselt numbers are functions of 12 parameters, 11 of which are identical in both the heat-transfer and mass-transfer numbers. The parameters ψ and χ are similar to the parameters Z and α given in the equations of references 1 and 2.

APPENDIX C

THEORY OF SELF-IGNITION OF SINGLE DROPLETS IN HOT AIR

According to current theories, ignition of a fuel-air mixture occurs in the vapor phase at a mixture ratio and temperature suitable for combustion. For a single droplet surrounded by a large amount of air this air-vapor mixture can be formed only in the film surrounding the liquid droplet. The temperature and mixture ratio at any point in the air-vapor film is controlled by the rates of heat and mass transfer and therefore by the temperature and mass histories of the droplet.

The spherically symmetrical model given in reference 1 is used to calculate the physical delay time. The temperature in the air-vapor film increases from the liquid temperature T_L at the liquid surface to the air temperature T_B at some distance from the drop. The partial pressure of the fuel vapor decreases from P_{fL} (the vapor pressure at the liquid surface) to zero at some distance from the drop. The curve of temperature against distance from the drop can be determined from the following equation for heat transfer as given in reference 1:

$$Q_v = K_m 4\pi r^2 \frac{dT}{dr} - wc_{pf}(T - T_L)$$

or

$$\frac{dT}{dr} = \frac{Q_v + wc_{pf}(T - T_L)}{K_m 4\pi r^2} \tag{C1}$$

The curve of partial pressure against distance can be determined from the following equations and identities as given in reference 2:

$$\frac{dP_f}{dr} = - \frac{RT}{DP_T} d_{v_f} r_o^2 \frac{P_a}{r^2} \tag{C2}$$

$$w = d_{v_f} M_f 4\pi r_o^2 \alpha \tag{C3}$$

$$\frac{dP_f}{dr} = - \frac{dP_a}{dr} \tag{C4}$$

Therefore,

$$\frac{dP_a}{dr} = \frac{RTwP_a}{DP_T M_f 4\pi r^2 \alpha} \tag{C5}$$

With the calculation technique of reference 1 it is possible to obtain temperature histories similar to those shown in figure 18. From these histories and equations (C1) and (C5) a relationship between the partial pressure of the fuel vapor and the temperature in the film is obtained. Illustrative partial pressure and temperature lines in the film are presented in figures 18(a) and 18(b).

If the partial pressure of the fuel vapor needed to form a combustible mixture is arbitrarily represented by the stoichiometric mixture, it is possible to determine the temperature of this mixture at any time. This mixture is represented by the horizontal line in figure 18(a). For the first curve drawn, the partial pressure of the liquid is below that needed to form the stoichiometric mixture. As the droplet heats up its vapor pressure rises and the point where the partial pressure in the film is such that a stoichiometric mixture is formed moves away from the liquid surface.

The temperature of the stoichiometric mixture as a function of distance in the film can be determined from figures 18(a) and 18(b). This temperature is plotted in figure 18(e). It should be noted that the temperature of the stoichiometric mixture increases with time. If conditions are right, the stoichiometric mixture reaches its self-ignition temperature before the droplet completely vaporizes and after a chemical delay the drop burns. The self-ignition temperature is represented by the dashed line of figure 18(e) which intersects the curve at point 2. This point then determines the physical-ignition-delay time as shown in figure 18(d). This is the earliest point in the vaporization process that a combustible mixture is formed at its self-ignition temperature.

The ignition delay θ_d is calculated by the following analytical technique: Combining equations (C1) and (C5) and using from reference 2

$$w = \frac{D}{RT_m} M_f A_o P_{fL} k_{Nu} \alpha$$

gives

$$\frac{dP_a}{dT} = \frac{K_m P_{fL} k_{Nu} P_a}{P_T\left(Q_v - wc_{pf}T_L + wc_{pf}T\right)} \tag{C6}$$

With the assumption that K_m and c_{pf} are constant at an average value throughout the film, the following substitution can be made:

$$C_1 = K_m P_{fL} k_{Nu} / P_T$$

$$C_2 = Q_v - wc_{pf} T_L$$

$$C_3 = wc_{pf}$$

The values of C_1, C_2, and C_3 are then constants throughout the film at any one instant of time. Equation (C6) becomes

$$\frac{dP_a}{P_a} = \frac{C_1 dT}{C_2 + C_3 T} \tag{C7}$$

Integrating between the limits $P_a(r) = P_T - P_f$ and $P_{a_{(r=\infty)}} = P_T$ where $T(r) = T$ and $T_{(r=\infty)} = T_B$,

$$T = \left(\frac{C_1}{C_2} + T_B\right)\left(1 - \frac{P_f}{P_T}\right)^{C_2/C_1} - \frac{C_2}{C_3} \tag{C8}$$

This equation relates the temperature T at some point in the air-vapor film to the vapor pressure P_f at the same point. This equation can be solved only in conjunction with the vaporization histories obtained by the technique described in reference 1, since the constants C_1, C_2, and C_3 are functions of the vaporization history.

The partial pressure of any fuel corresponding to a given mixture strength (on a weight basis) is determined by the following equation

$$P_f = \frac{P_T}{\frac{M_f}{M_a}\frac{1}{y} + 1} \tag{C9}$$

Although it is possible to burn air-vapor mixtures over a range of mixture ratios, a stoichiometric mixture has been chosen to represent the combustible mixture.

A representative history of a drop of n-decane calculated by the technique of reference 1 and equations (C8) and (C9) is shown in figure 19. At point a the liquid temperature has reached the value where the liquid vapor pressure is just high enough to form the stoichiometric mixture. From this point the temperature of the stoichiometric mixture rises and approaches a constant value as the droplet approaches the steady-state temperature.

Sometime along the path of the stoichiometric-mixture-temperature line a point is reached at which the temperature equals the self-ignition temperature. The self-ignition temperatures of pure hydrocarbons are found in the literature (among others, refs. 7, 8, and 9). The values obtained by different investigators vary according to the procedure, container, and purity of the hydrocarbon. The values given in reference 7 were used in this investigation although they are lower than those given by other investigators. The self-ignition temperature of the stoichiometric mixture is reached at point b in figure 19 and can be taken as the dividing point between the physical and chemical ignition delays of a single droplet.

APPENDIX D

ADIABATIC SATURATION IN SPRAYS

If fuel is injected in the form of a spray in an airstream, the static pressure change in the system due to vaporization cooling is very small. If no heat is transferred from adjacent segments in the spray and sufficient time is allowed, the temperature of any segment will ultimately reach equilibrium. Two different cases may arise depending upon the overall fuel-air ratio. For rich mixtures the equilibrium will occur in the wet region; that is, a three-phase system will result. In the case of leaner mixtures all of the fuel will vaporize and the vapor will be superheated to the equilibrium temperature.

The wet region is defined as the condition where the equilibrium vapor-air ratio is less than or equal to the overall fuel-air ratio. For the wet region the heat balance may be written

$$Q = Q_r + Q_\lambda .$$

The following equation can then be written for a constant-pressure system:

$$\int_{T_2}^{T_{B1}} c_{pa}\, dT = y \int_{T_{L1}}^{T_2} c_{pL}\, dT + \left(\frac{P_{fL2}}{P_T - P_{fL2}}\right) \frac{M_f}{M_a} \lambda_L \qquad (D1)$$

For the case where no liquid remains at the equilibrium region the following equation applies:

$$\int_{T_2}^{T_{B1}} c_{pa}\, dT = y \left(\int_{T_{L2}}^{T_i} c_{pL}\, dT + \lambda_i + \int_{T_i}^{T_2} c_{pf}\, dT \right) \qquad (D2)$$

where T_i is an intermediate temperature at which the liquid is assumed to be completely vaporized at a pressure equal to the partial pressure of the completely vaporized fuel in the system. Equations (D1) and (D2) may be solved to obtain the final adiabatic equilibrium temperature for any fuel-air ratio and initial conditions.

While the above theory gives the conditions at equilibrium, it gives no information concerning what is happening in the spray as a function of time.

In order to determine the time dependency, consider a spray of uniform drop size or some section of a spray where drop size is assumed uniform. Also assume that there is no net mass or heat transfer to or from this section. The approximation will be made that all concentration and temperature gradients are confined to films of small but finite width surrounding each drop. Air and fuel vapor outside the film boundaries will be considered uniform throughout the section and will be referred to as the "atmosphere." It is further assumed that the droplets within the section have the same velocity relative to the atmosphere; this velocity may be constant or varying in time. For convenience one may think of each drop affecting only a volume of air determined by the overall air-fuel ratio (by weight). The temperature and composition of the atmosphere as a function of time may thus be determined, taking into account the effect of the heat and mass transfer on the temperature and fuel partial pressure in the atmosphere. Extensive variables for the spray section may obviously be obtained by merely multiplying the single-drop results by the total number of drops.

The mass-transfer equation given in reference 2 may be written as

$$d_{v_f} = \frac{DP_T}{RT}\left(\frac{1}{B_o} + \frac{1}{r_o}\right) \log_e\left(\frac{P_a B}{P_a L}\right) \tag{D3}$$

The pressure P_{fB} can then be written as

$$P_{fB} = \frac{P_T}{\left(\frac{\overline{W_a}\, W_f}{\overline{W_f}\, W_a}\right) + 1} \tag{D4}$$

Clearly,

$$\overline{W_a} = M_{to}/y$$

$$\overline{W_f} = \sum_{i=1}^{n} w_i\, \Delta t_i$$

Then

$$d_{v_f} = - \frac{D}{RT_m}\left(\frac{1}{B_o} + \frac{1}{r_o}\right)\left(P_{fL} - P_{fB}\right)\alpha' \tag{D5}$$

where

$$\alpha' = \left(\frac{P_T}{P_{fL} - P_{fB}}\right)\log_e\left(\frac{P_T - P_{fB}}{P_T - P_{fL}}\right) \tag{D6}$$

As in reference 2 the mass-transfer equation may be written as

$$w = Ak\left(P_{fL} - P_{fB}\right)\alpha' \tag{D7}$$

where $\left(P_{fL} - P_{fB}\right)$ is now the reduced driving force.

As the drop vaporizes the atmosphere is cooled and thus the average temperature of the atmosphere T_B must be calculated for each increment of time. The heat supplied by the atmosphere is the heat that enters the outer edge of the vapor film:

$$Q = Q_L + Q_s$$

If the mass of air in the film is considered negligible Q_s is the heat that goes into superheating the fuel vapor in the film. Therefore, for any time increment Δt_n

$$T_{B(n+1)} = T_{Bn} - \left[\frac{Q_L + w\left(T_B - T_L\right)}{\overline{W}_a c_{pa} + \overline{W}_f c_{pf}}\right]_n \Delta t_n \tag{D8}$$

The stepwise technique described in reference 1 may then be used to solve the vaporization equations. The vaporization histories must of course predict a final temperature for the system that agrees with the final temperatures as calculated by the thermodynamic theory presented earlier.

Histories using this technique are shown in figures 17(a) and 17(b).

REFERENCES

1. El Wakil, M. M., Uyehara, O. A., and Myers, P. S.: A Theoretical Investigation of the Heating-Up Period of Injected Fuel Droplets Vaporizing in Air. NACA TN 3179, 1954.

2. El Wakil, M. M., Priem, R. J., Brikowski, H. J., Myers, P. S., and Uyehara, O. A.: Experimental and Calculated Temperature and Mass Histories of Vaporizing Fuel Drops. NACA TN 3490, 1956.

3. El Wakil, M. M., Uyehara, O. A., and Myers, P. S.: Fuel Vaporization and Ignition Lag in Diesel Combustion. SAE Jour., vol. 64, 1956, pp. 712-729. Paper presented at Nat. Diesel Meeting of S.A.E., St. Louis, Mo., Nov. 1955.

4. Hirschfelder, Joseph O., Curtiss, Charles F., and Bird, R. Byron: Molecular Theory of Gases and Liquids. John Wiley & Sons, Inc., 1954.

5. Schlichting, Hermann (J. Kestin, trans.): Boundary Layer Theory. McGraw-Hill Book Co., Inc., 1955.

6. Fluid Motion Panel of the Aeronautical Research Committee and Others (S. Goldstein, ed.): Modern Developments in Fluid Dynamics. Vol. II. The Clarendon Press (Oxford), 1938.

7. Frank, Charles E., and Blackham, Angus U.: Investigation of Hydrocarbon Ignition. NACA TN 2549, 1952.

8. Jackson, Joseph L.: Spontaneous Ignition Temperatures of Pure Hydrocarbons and Commercial Fluids. NACA RM E50J10, 1950.

9. Sortman, C. W., Beatty, H. A., and Heron, S. D.: Spontaneous Ignition of Hydrocarbons. Ind. and Eng. Chem., vol. 33, no. 3, Mar. 1941, pp. 357-360.

10. Godsave, G. A. E.: The Burning of Single Drops of Fuel. Nat. Gas Turbine Establishment, Report No. R.125. Part IV. The Flow of Heat and Carbon Residue Formation in Drops of Fuel.

11. Aarnes, M. N.: Physical and Chemical Delay of Pure Hydrocarbons Auto-Igniting in a Combustion Bomb. M. S. Thesis, Univ. of Wisc., 1954.

12. Ingebo, Robert D.: Vaporization Rates and Drag Coefficients for Isooctane Sprays in Turbulent Air Streams. NACA TN 3265, 1954.

13. Jost, Wilhelm (Huber O. Croft, trans.): Explosion and Combustion Processes in Gases. McGraw-Hill Book Co., Inc., 1946.

14. Maxwell, J. B.: Data Book on Hydrocarbons. D. Van Nostrand Co., Inc., 1950.

15. Anon.: Selected Values of Properties of Hydrocarbons. Res. Proj. 44, A.P.I. and Nat. Bur. Standards, July 1949.

16. Ingebo, Robert D.: Vaporization Rates and Heat-Transfer Coefficients for Pure Liquid Drops. NACA TN 2368, 1951.

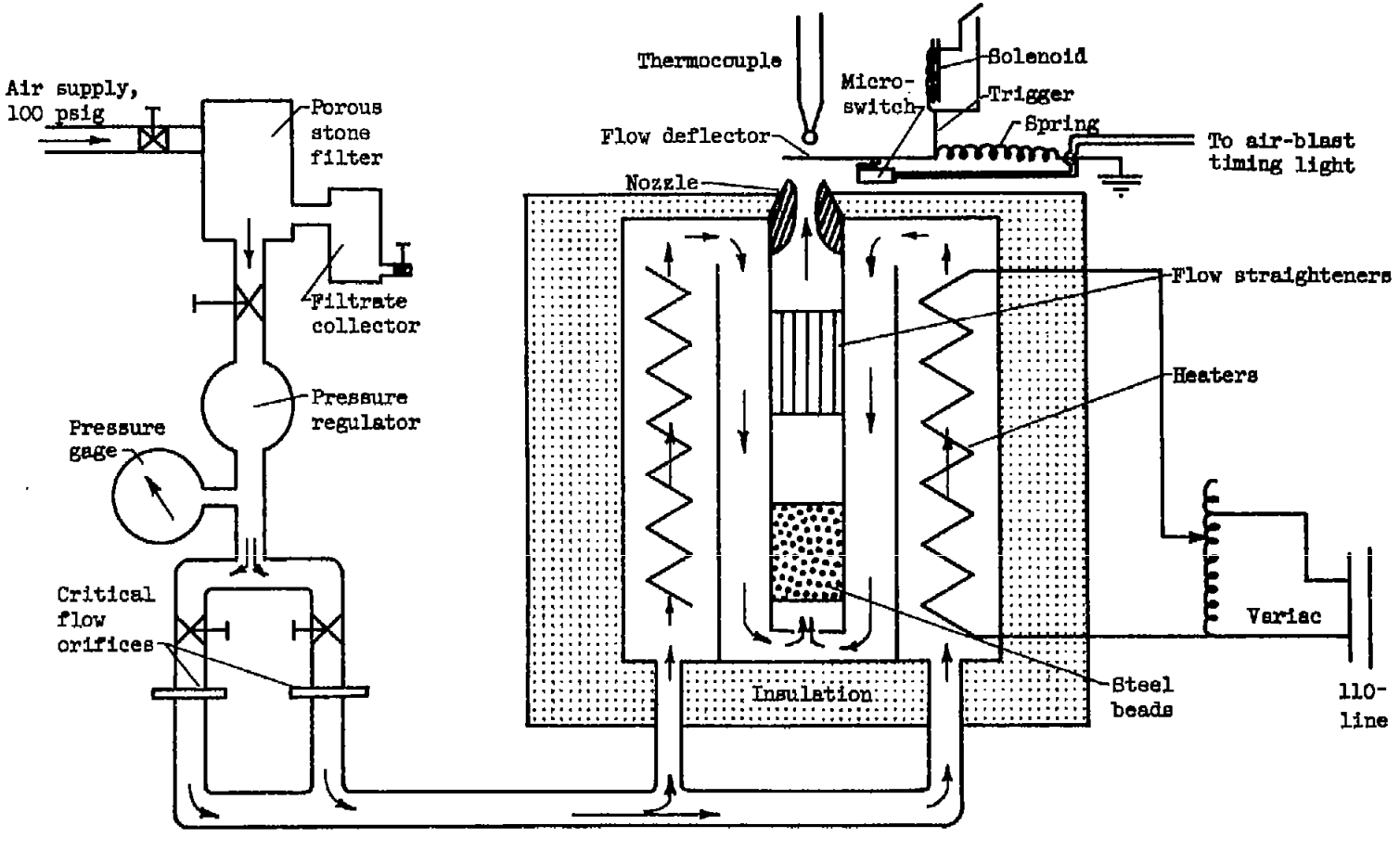

Figure 1.- Schematic diagram of experimental apparatus.

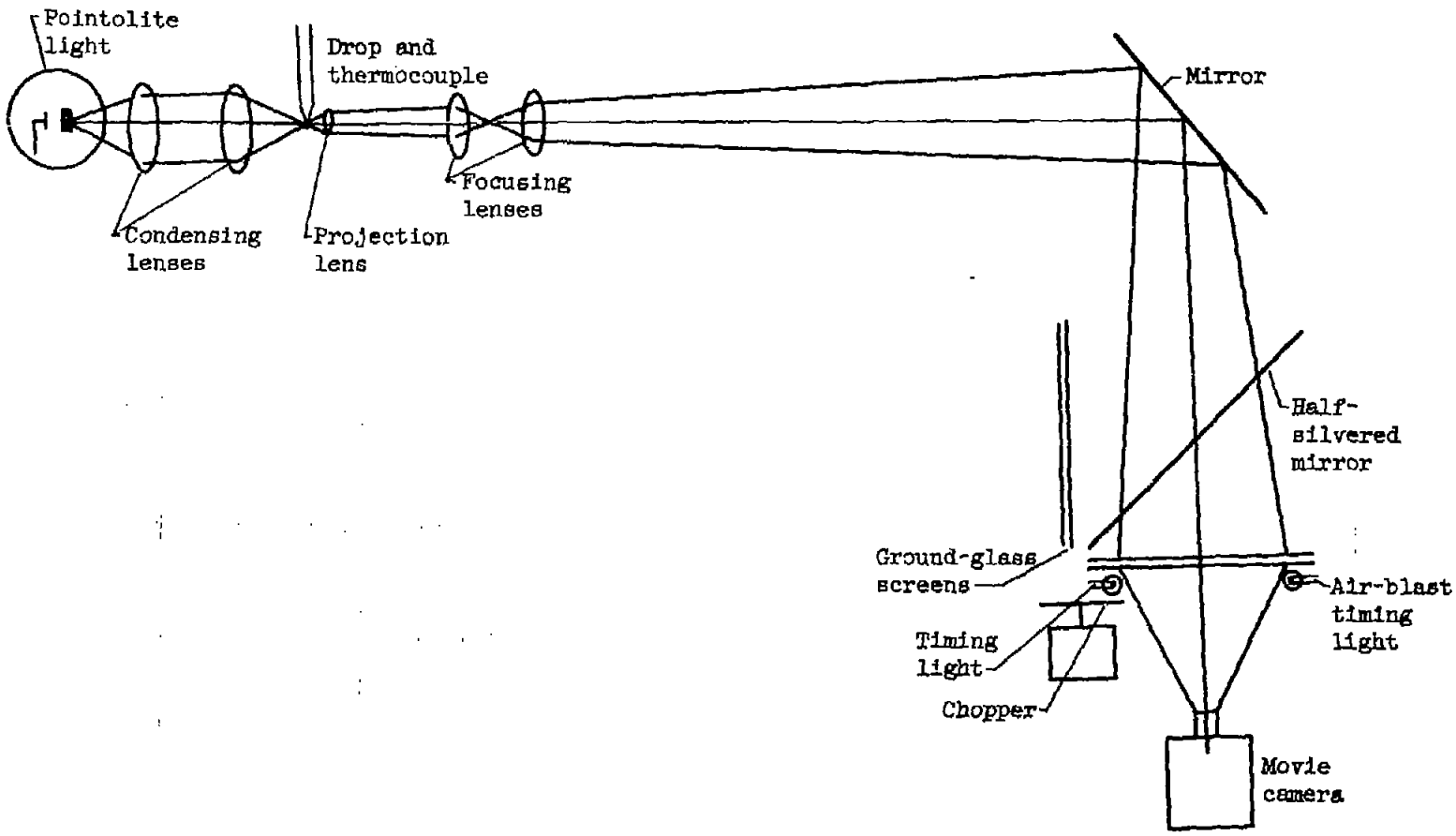

Figure 2.- Schematic diagram of optical system.

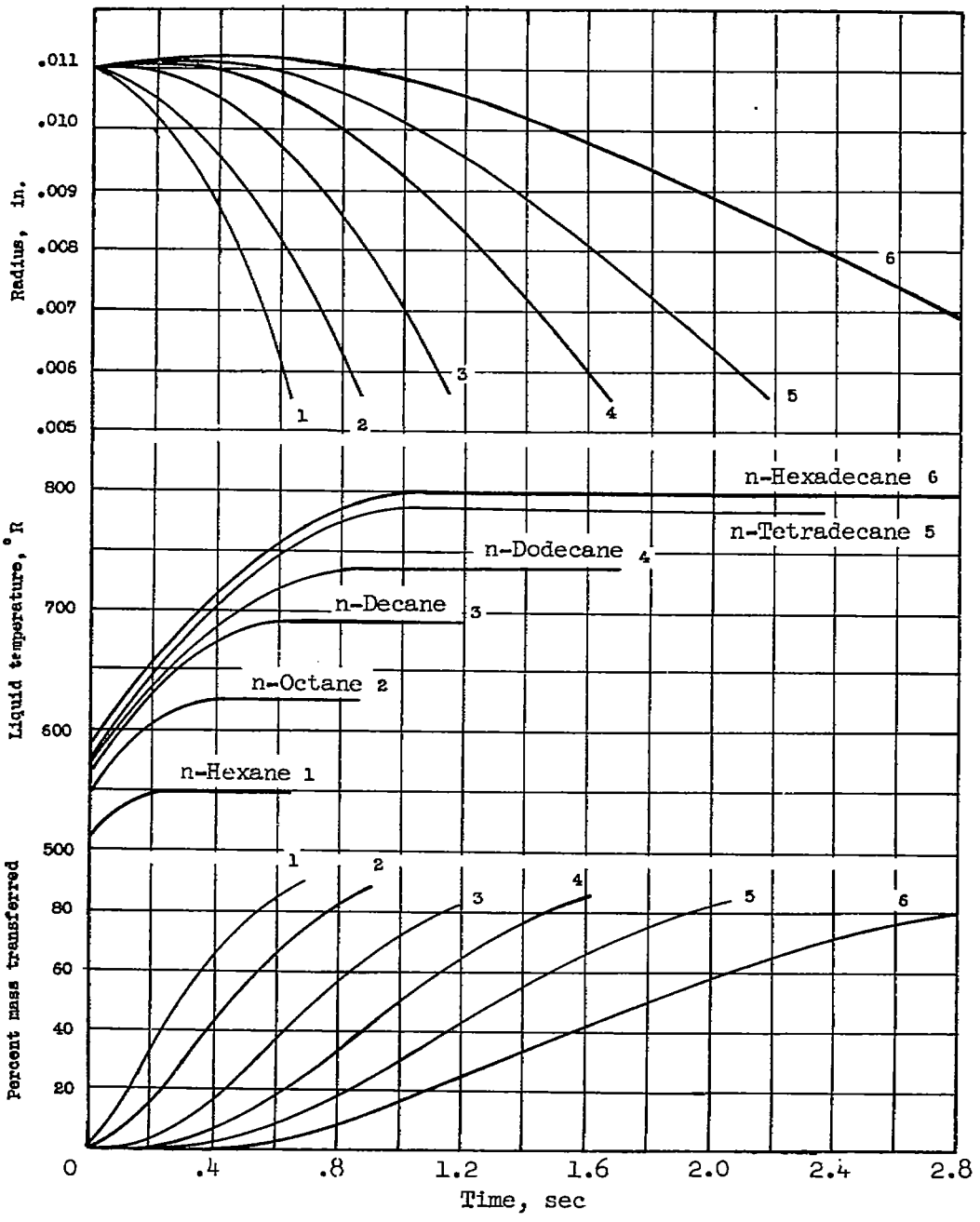

(a) Air temperature, 835° R; air velocity, 82 inches per second; initial drop diameter, 550 microns.

Figure 3.- Radius, temperature, and mass histories of various fuels.

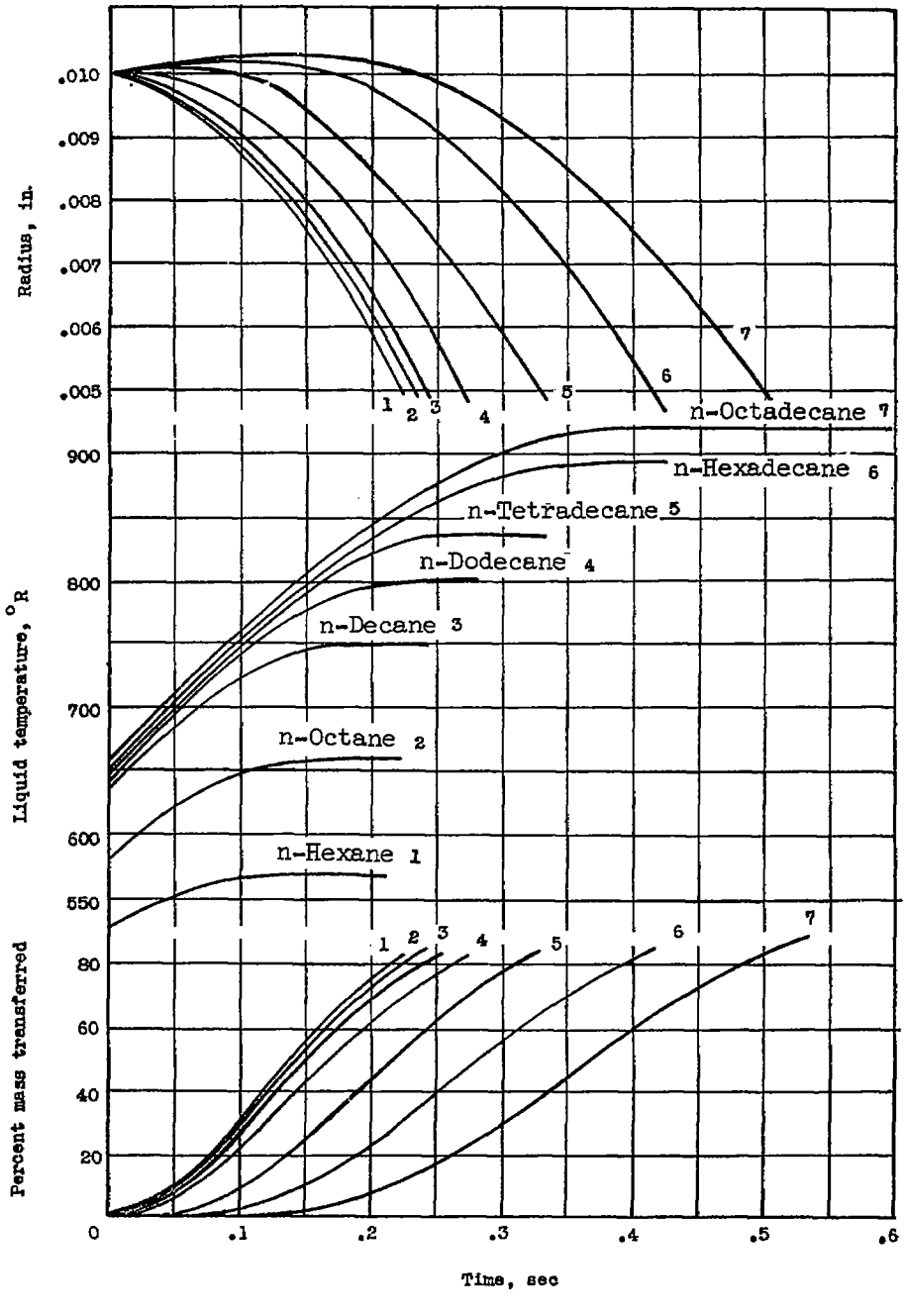

(b) Air temperature, 1360° R; air velocity, 102 inches per second; initial drop diameter, 500 microns.

Figure 3.- Concluded.

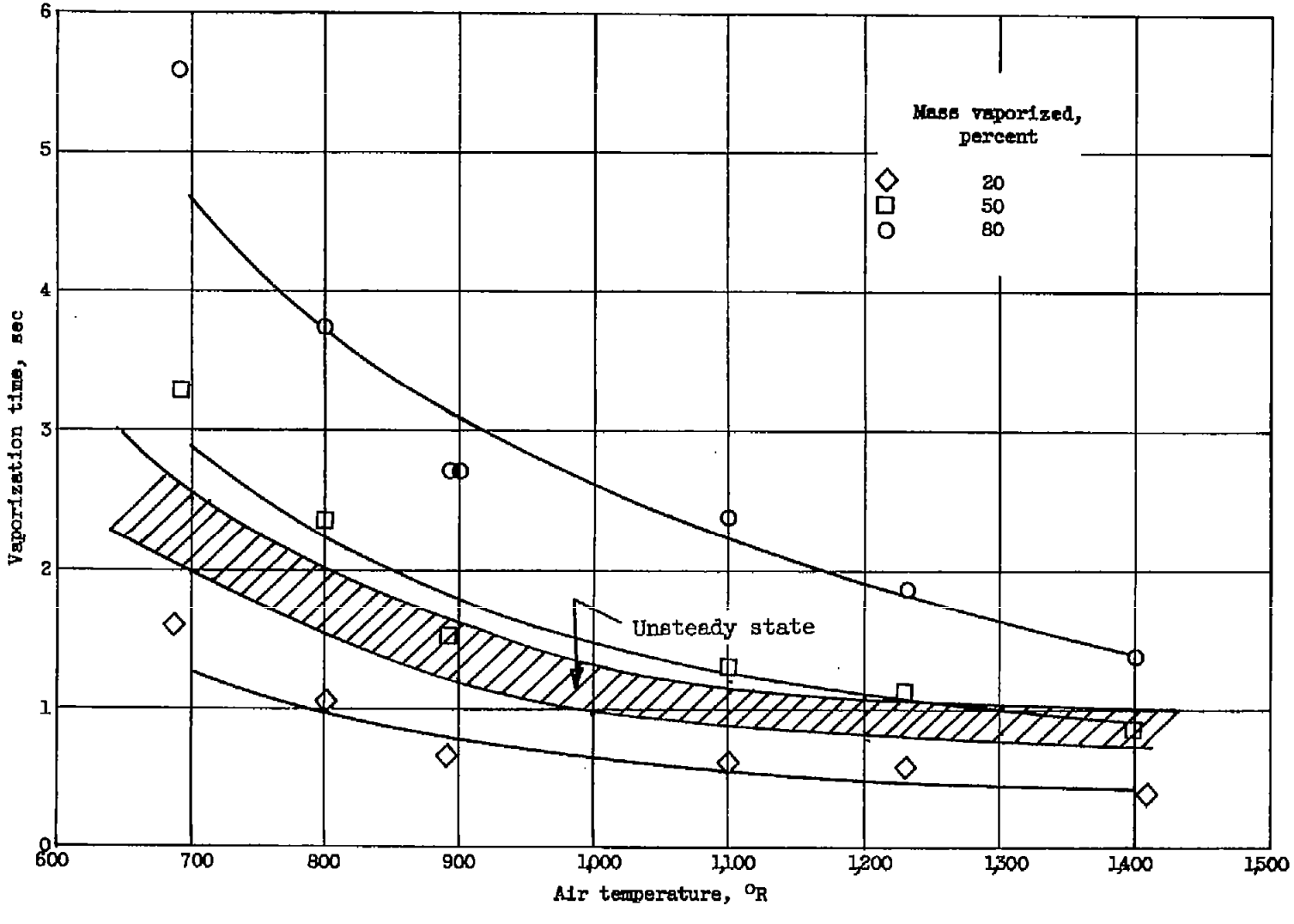

(a) n-hexane. Drop diameter, 1,600 microns; air velocity, 90 inches per second.

Figure 4.- Experimental vaporization time as a function of air temperature.

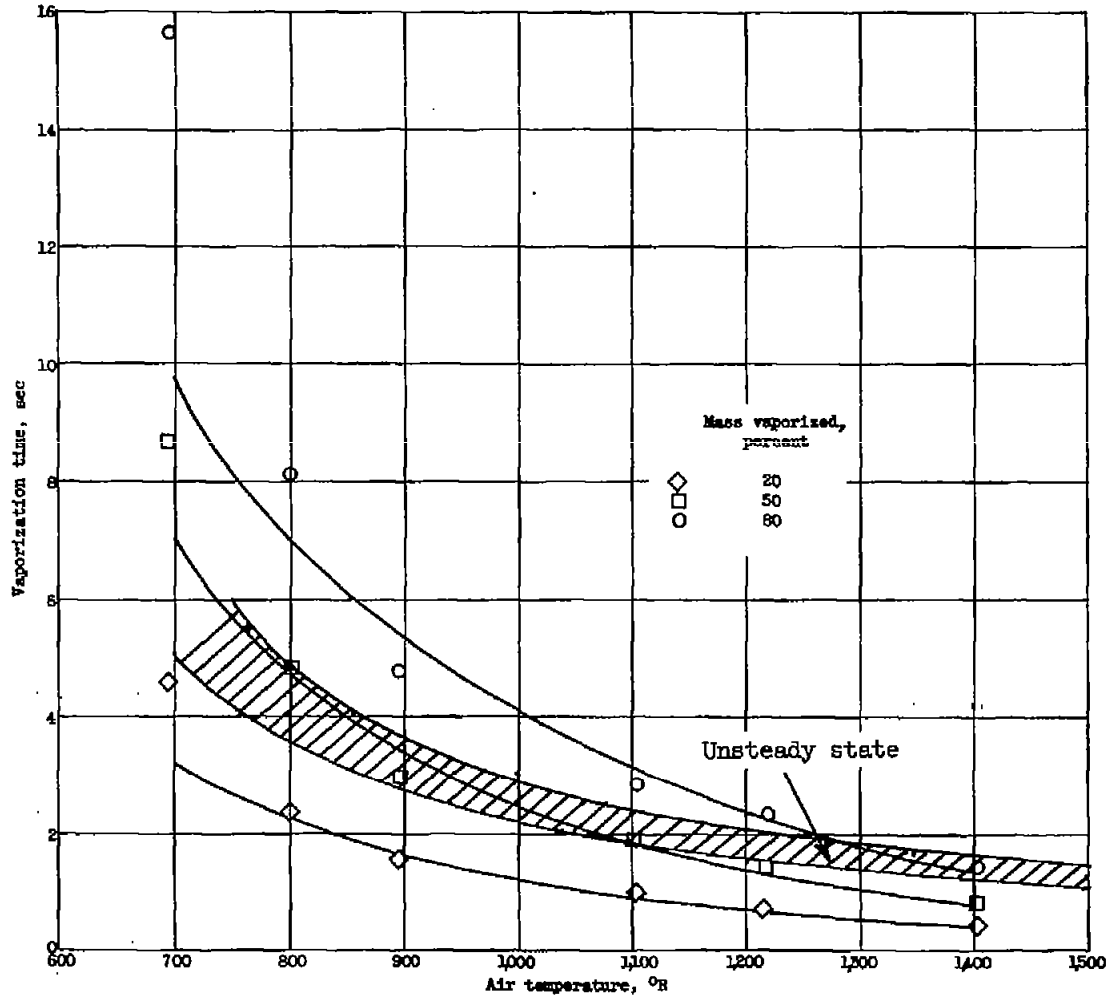

(b) n-decane. Drop diameter, 1,600 microns; air velocity, 90 inches per second.

Figure 4.- Continued.

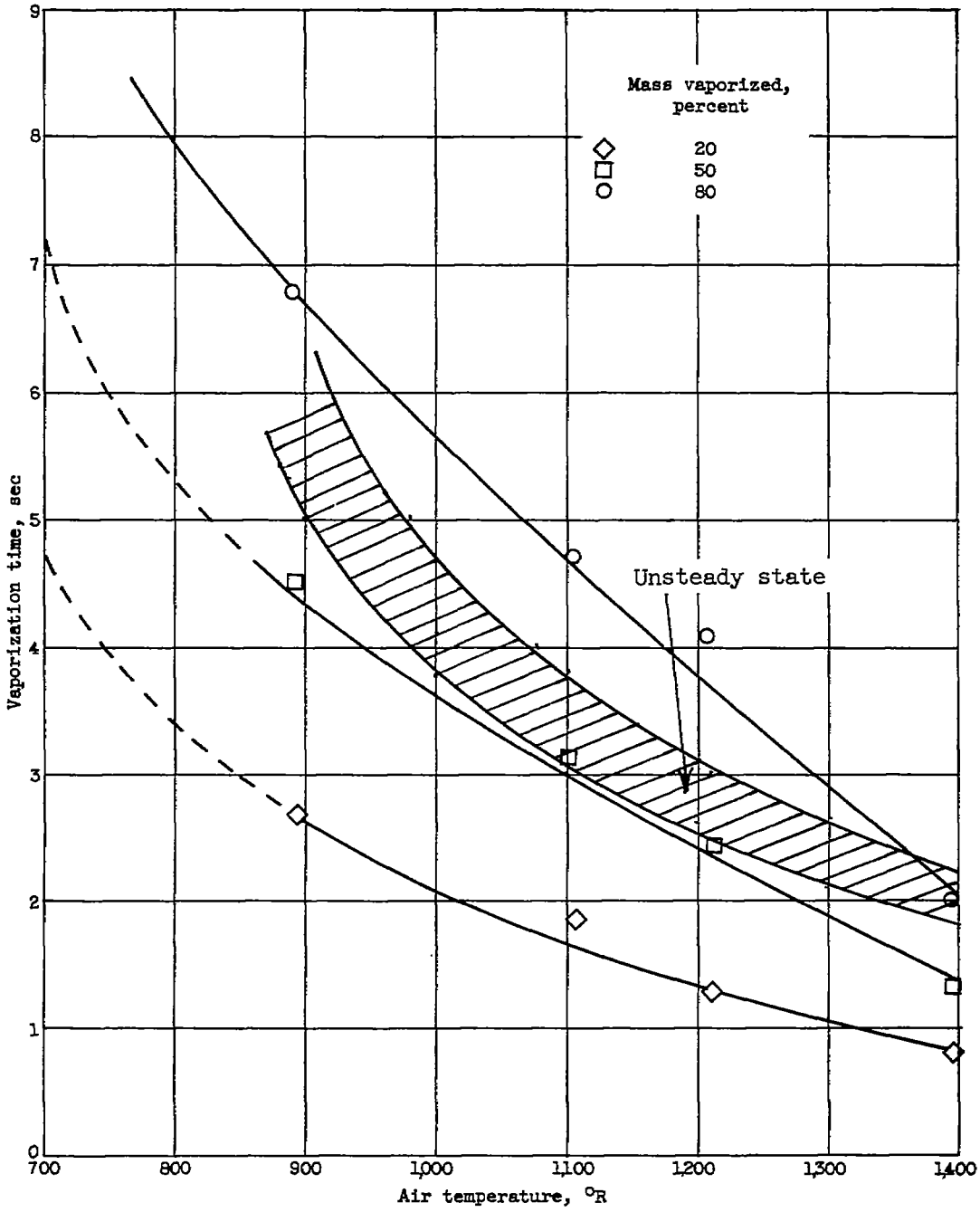

(c) n-hexadecane. Drop diameter, 1,600 microns; air velocity, 90 inches per second.

Figure 4.- Concluded.

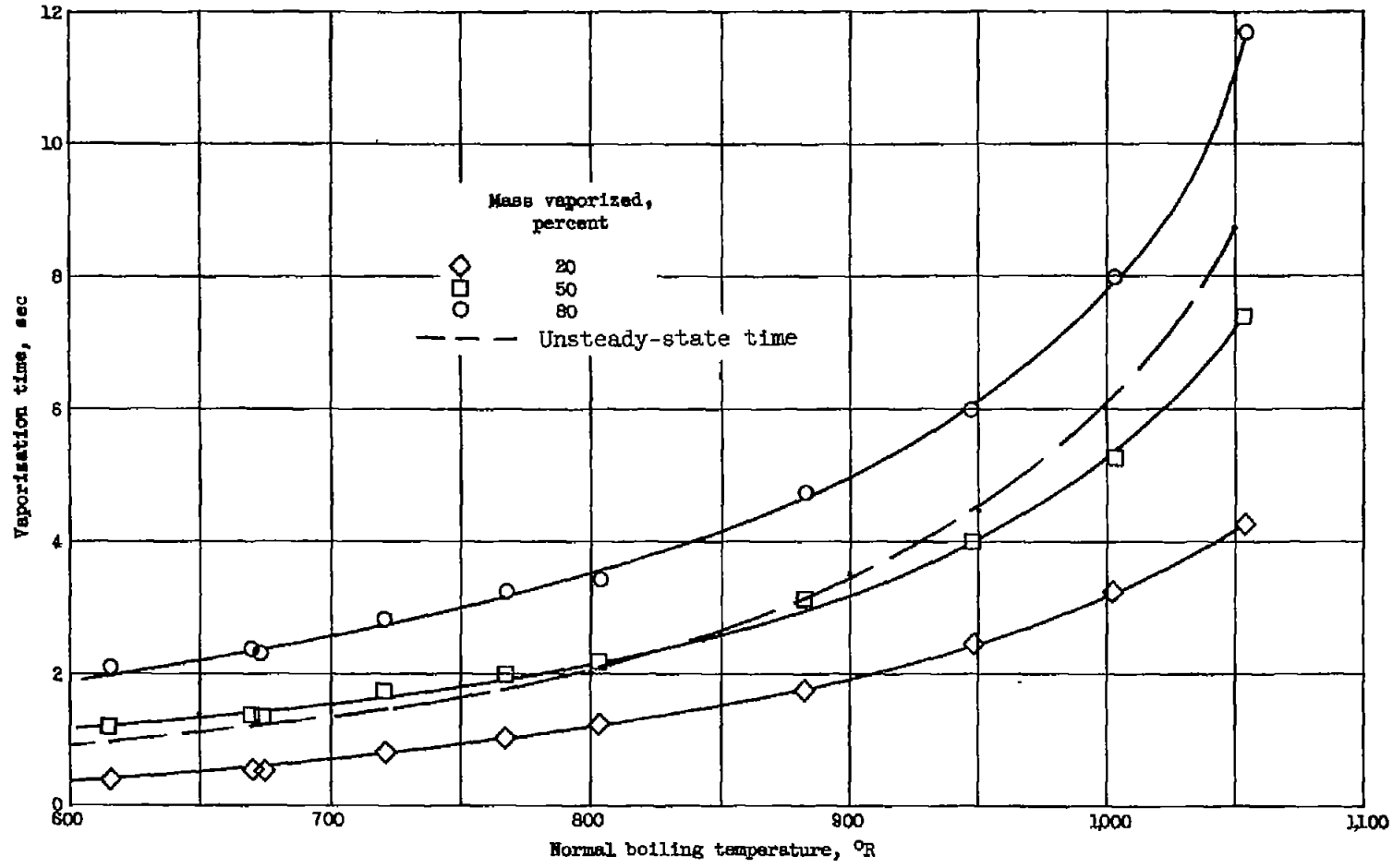

(a) Air temperature, 900° R; drop diameter, 1,600 to 1,700 microns; velocity, 80 inches per second.

Figure 5.- Experimental vaporization time as a function of normal boiling temperature for various fuels.

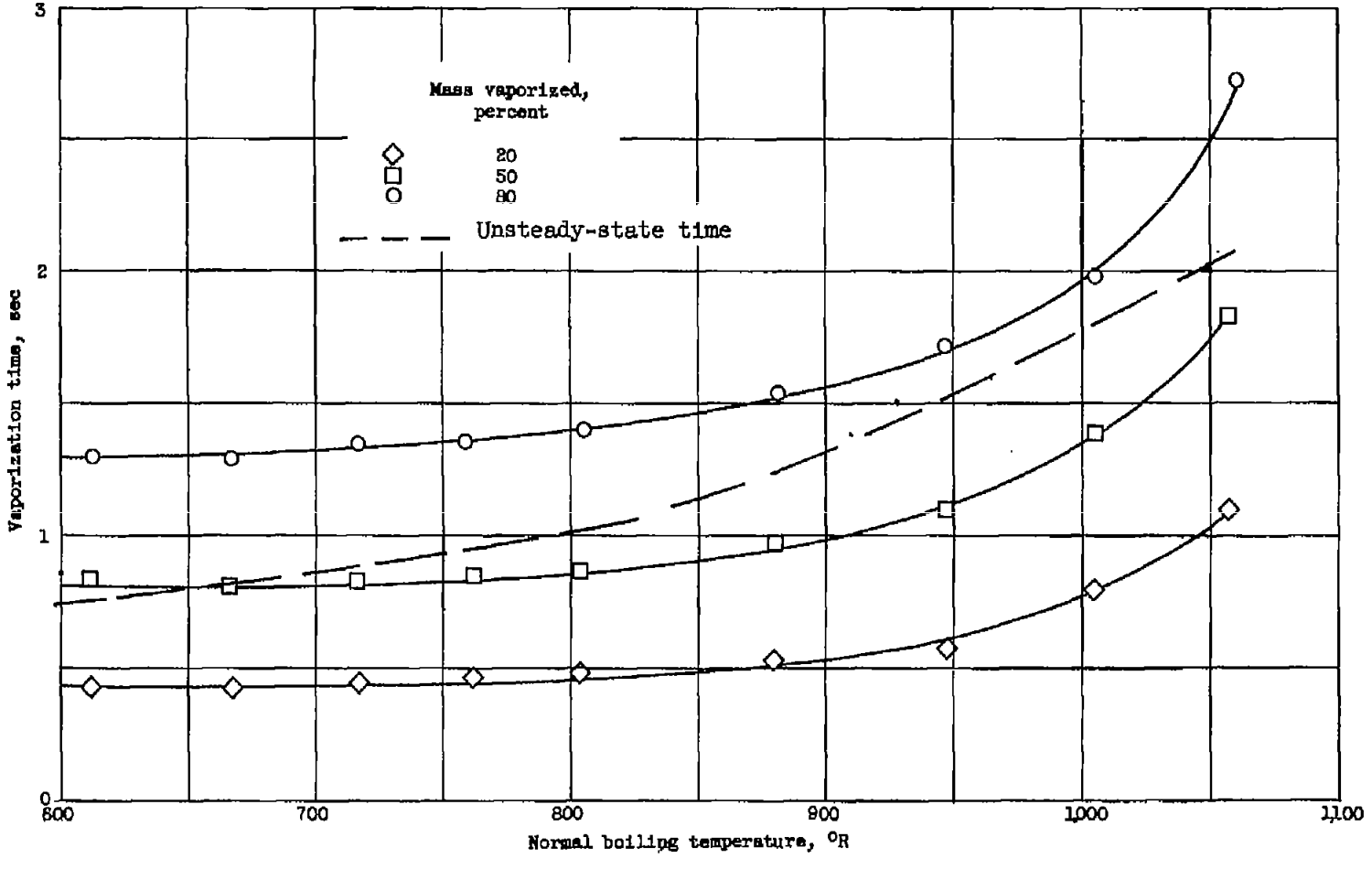

(b) Air temperature, 1,430° R; drop diameter, 1,500 to 1,600 microns; velocity, 80 inches per second.

Figure 5.- Concluded.

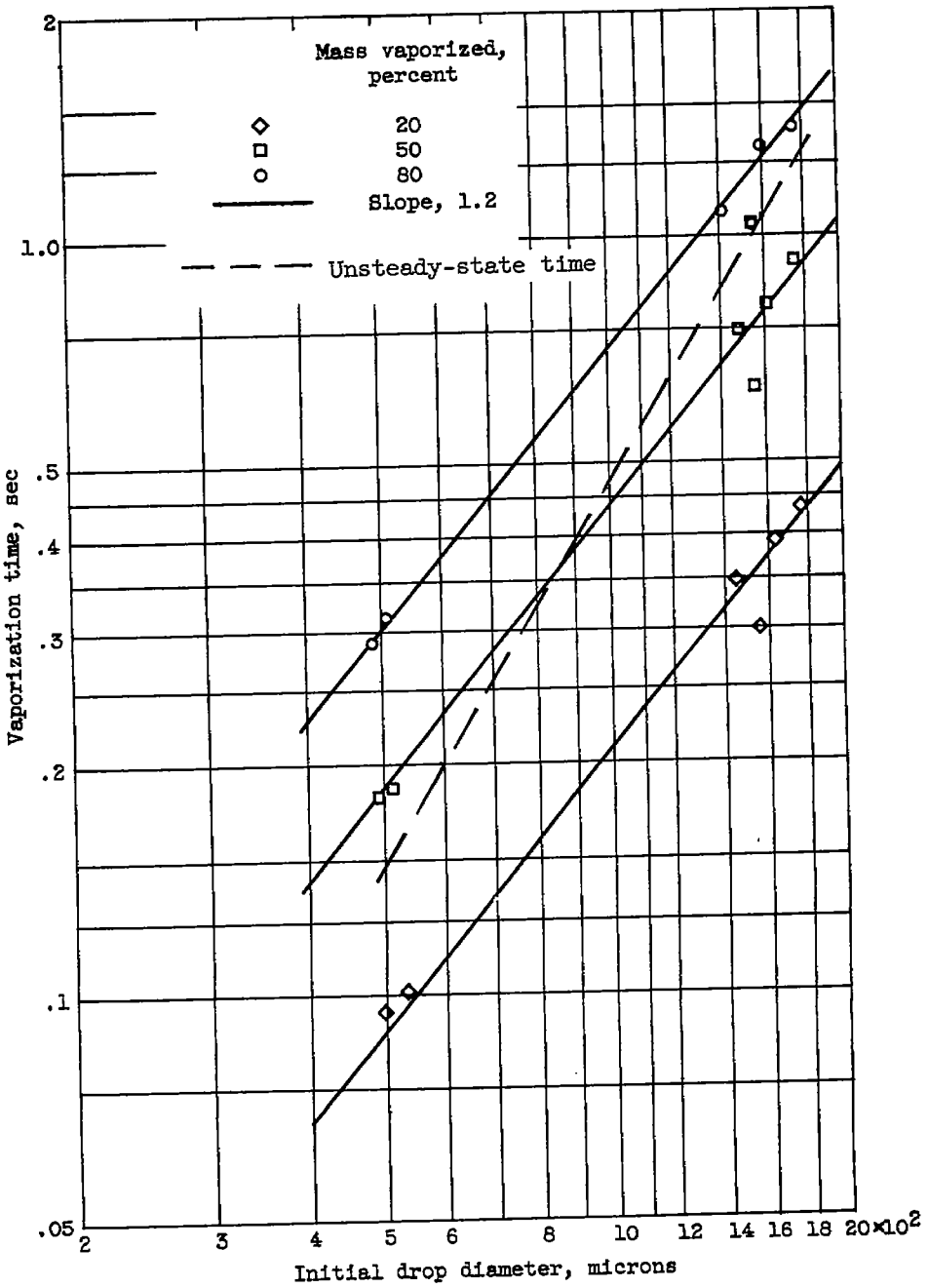

(a) n-hexane. Air temperature, 1,350° R; air velocity, 80 inches per second.

Figure 6.- Experimental vaporization time as a function of initial drop diameter.

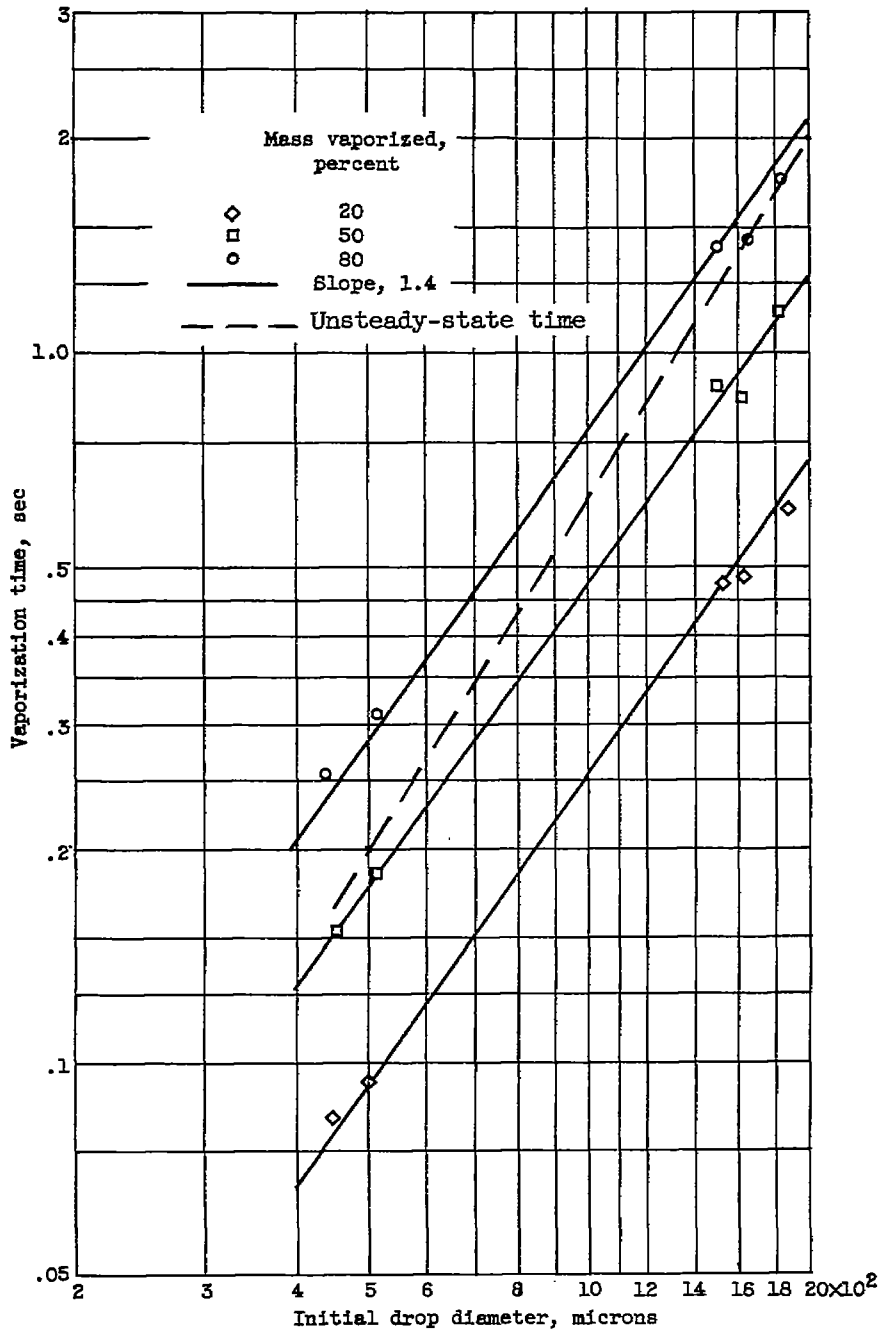

(b) n-decane. Air temperature, 1,350° R; air velocity, 80 inches per second.

Figure 6.- Continued.

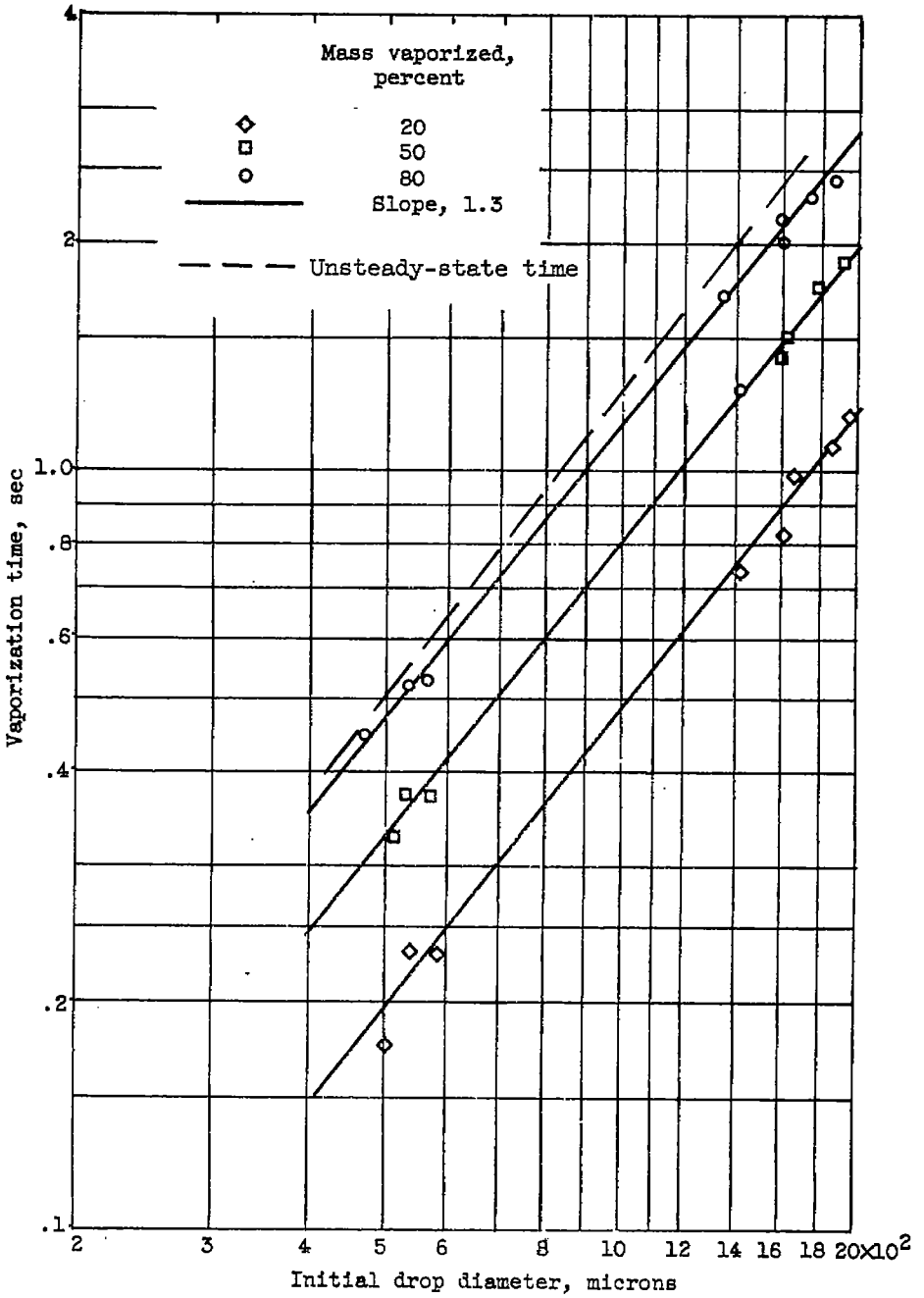

(c) n-hexadecane. Air temperature, 1,350° R; air velocity, 80 inches per second.

Figure 6.- Concluded.

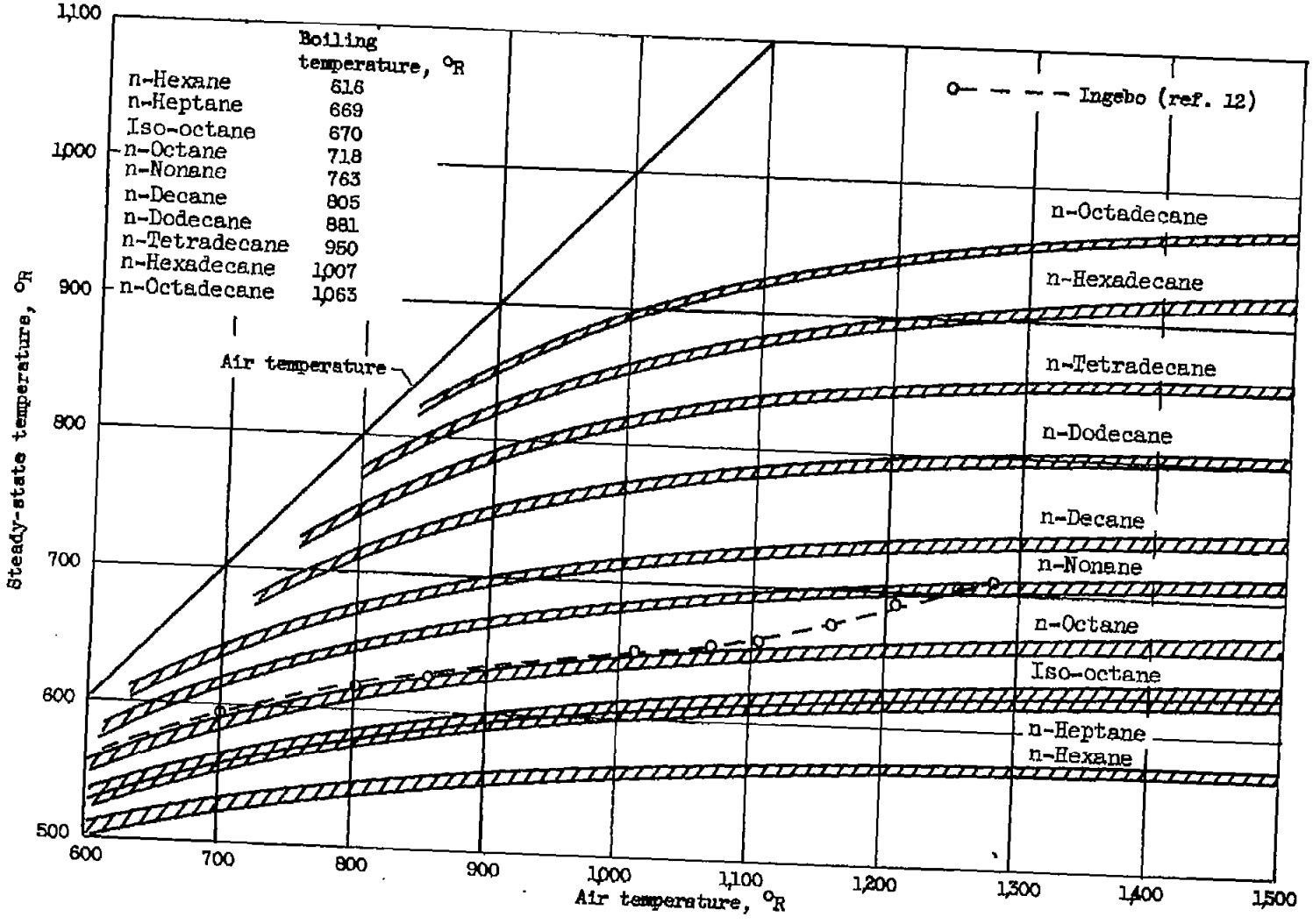

Figure 7.- Experimental steady-state temperature as a function of air temperature for various fuels.

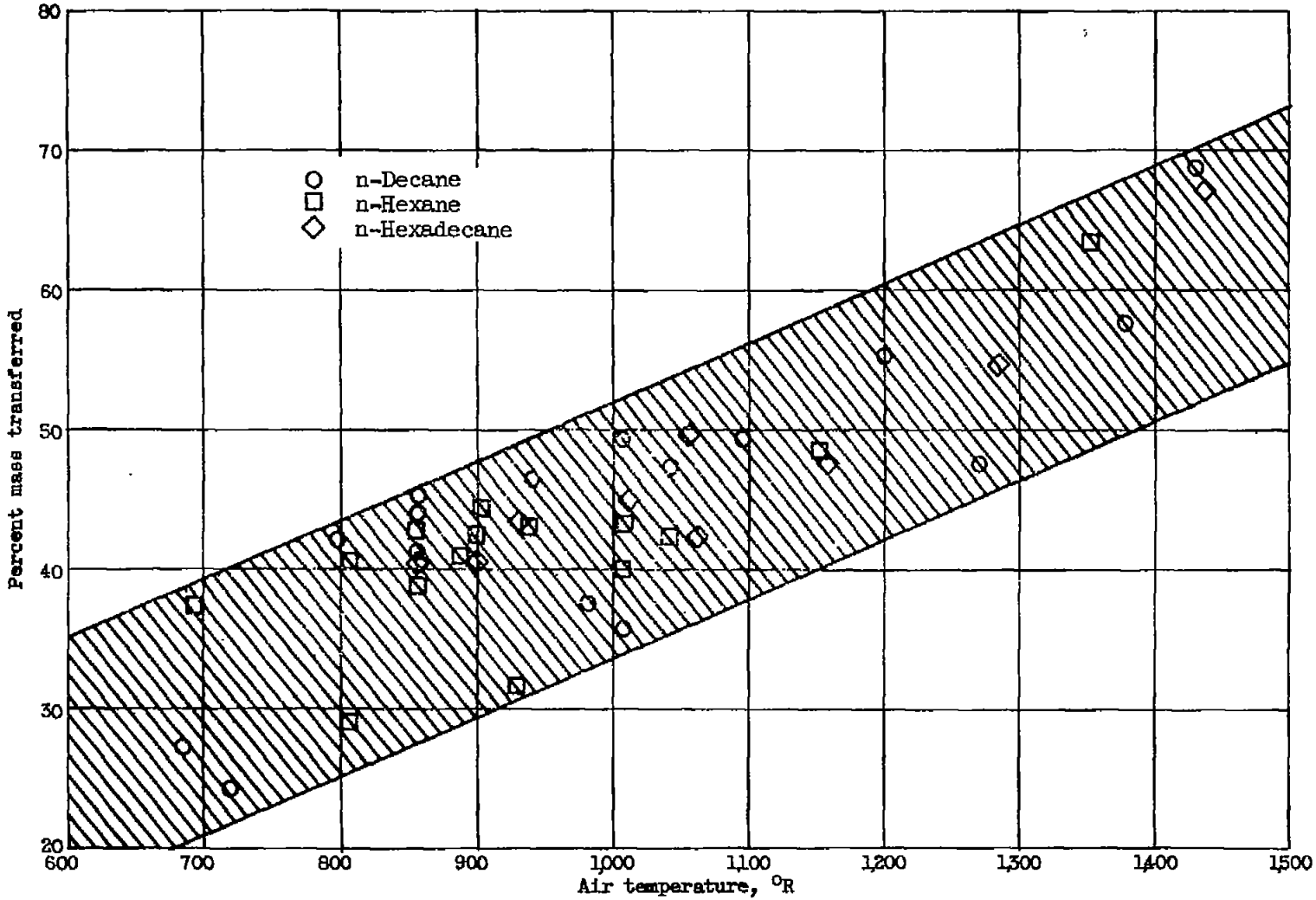

Figure 8.- Experimental percent mass transferred at end of unsteady state as a function of air temperature.

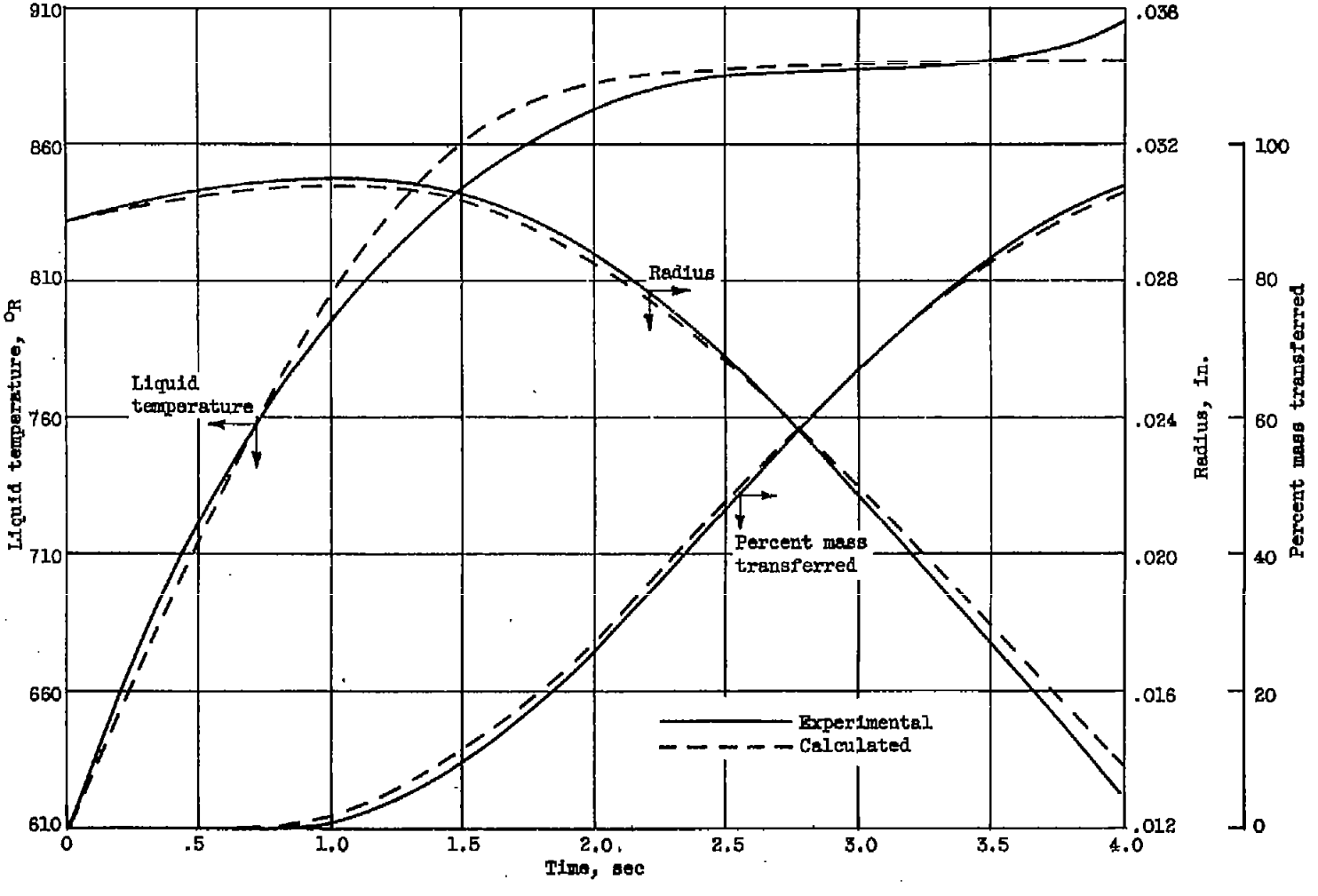

(a) n-hexadecane. Air temperature, 1,230° R; air velocity, .80 inches per second; initial diameter, 1,520 microns.

Figure 9.- Comparison of experimental and calculated histories of a droplet.

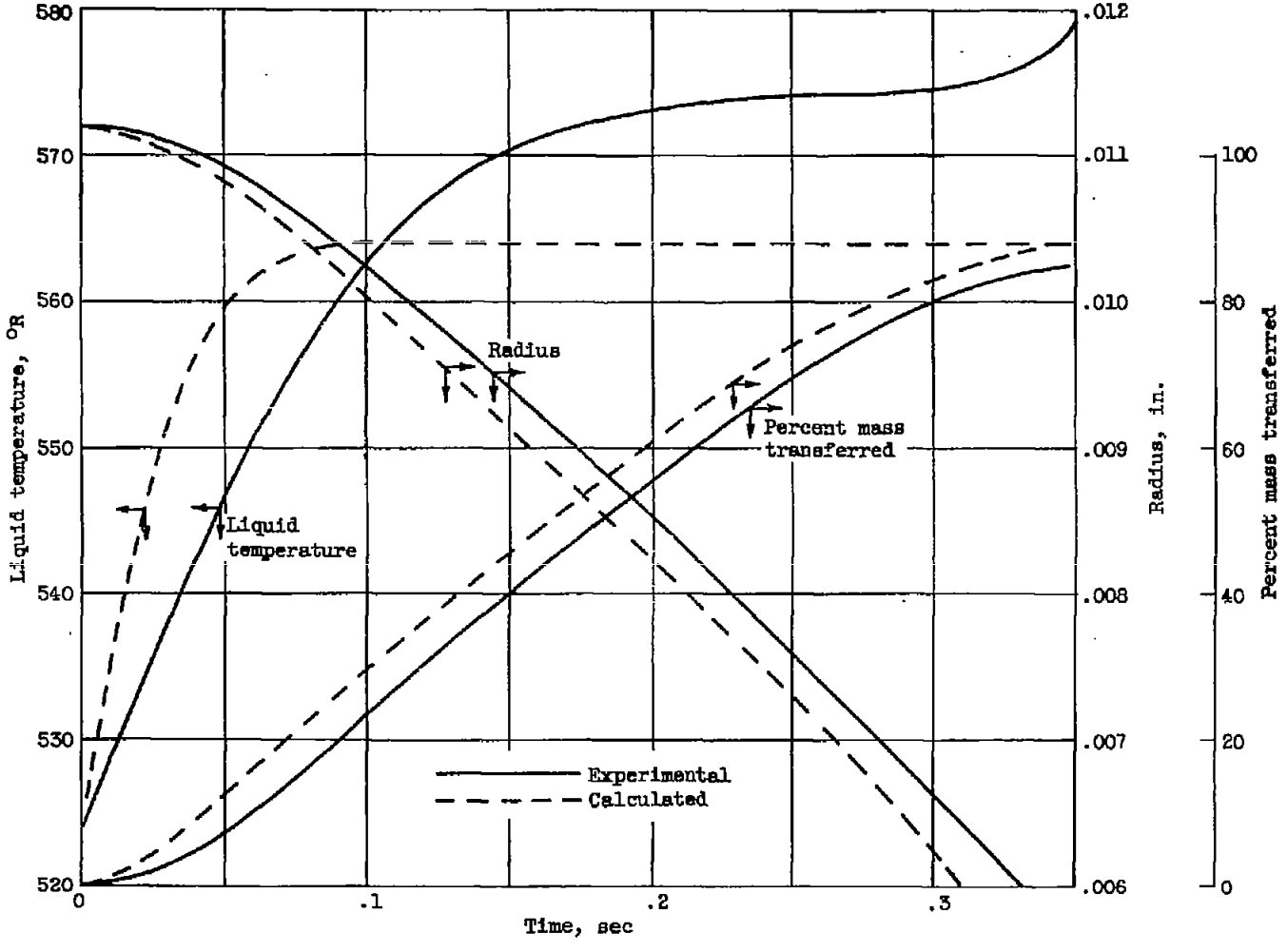

(b) n-hexane. Air temperature, 1,280° R; air velocity, 120 inches per second; initial diameter, 560 microns.

Figure 9.- Concluded.

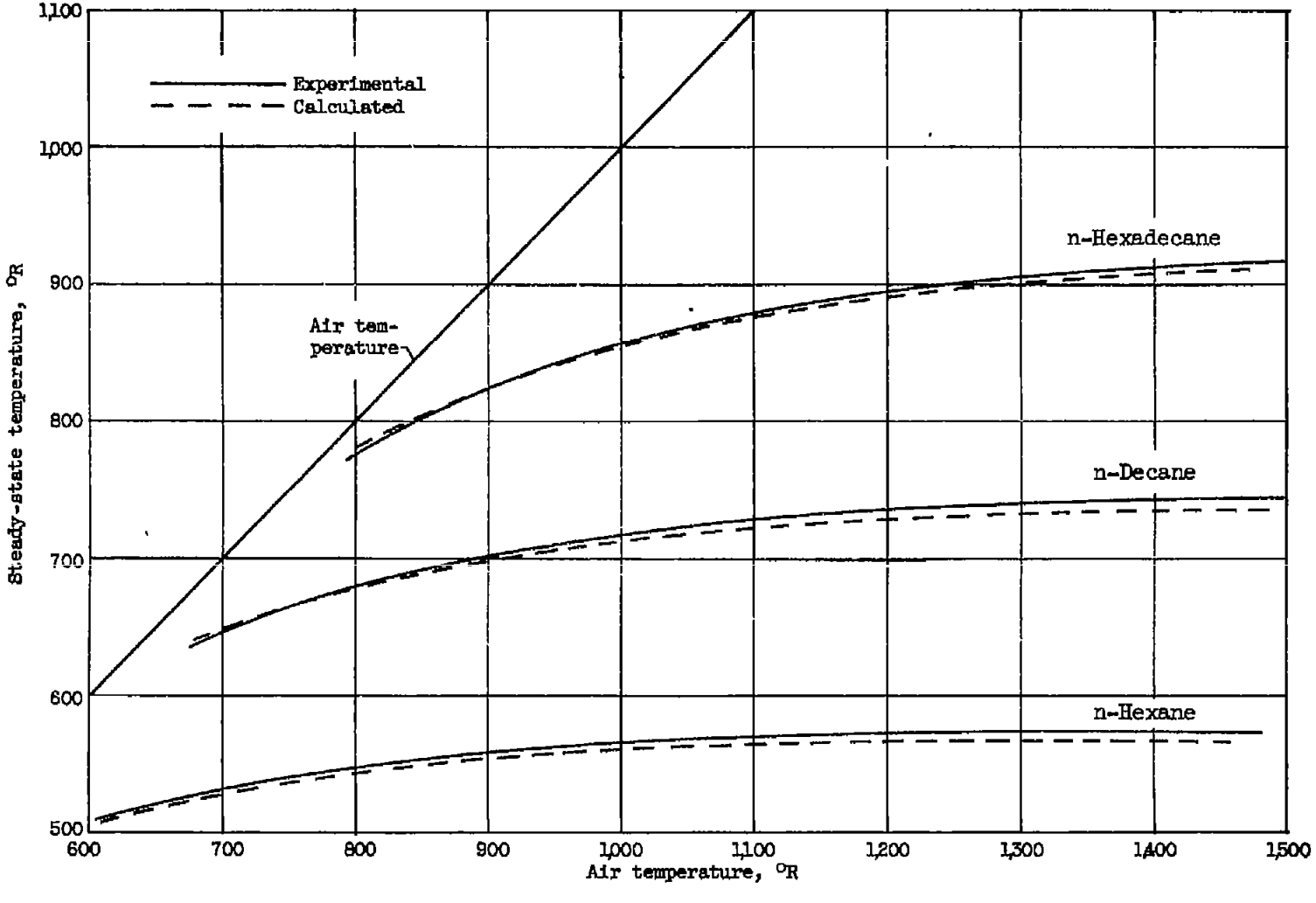

Figure 10.- Comparison of experimental and calculated steady-state temperatures.

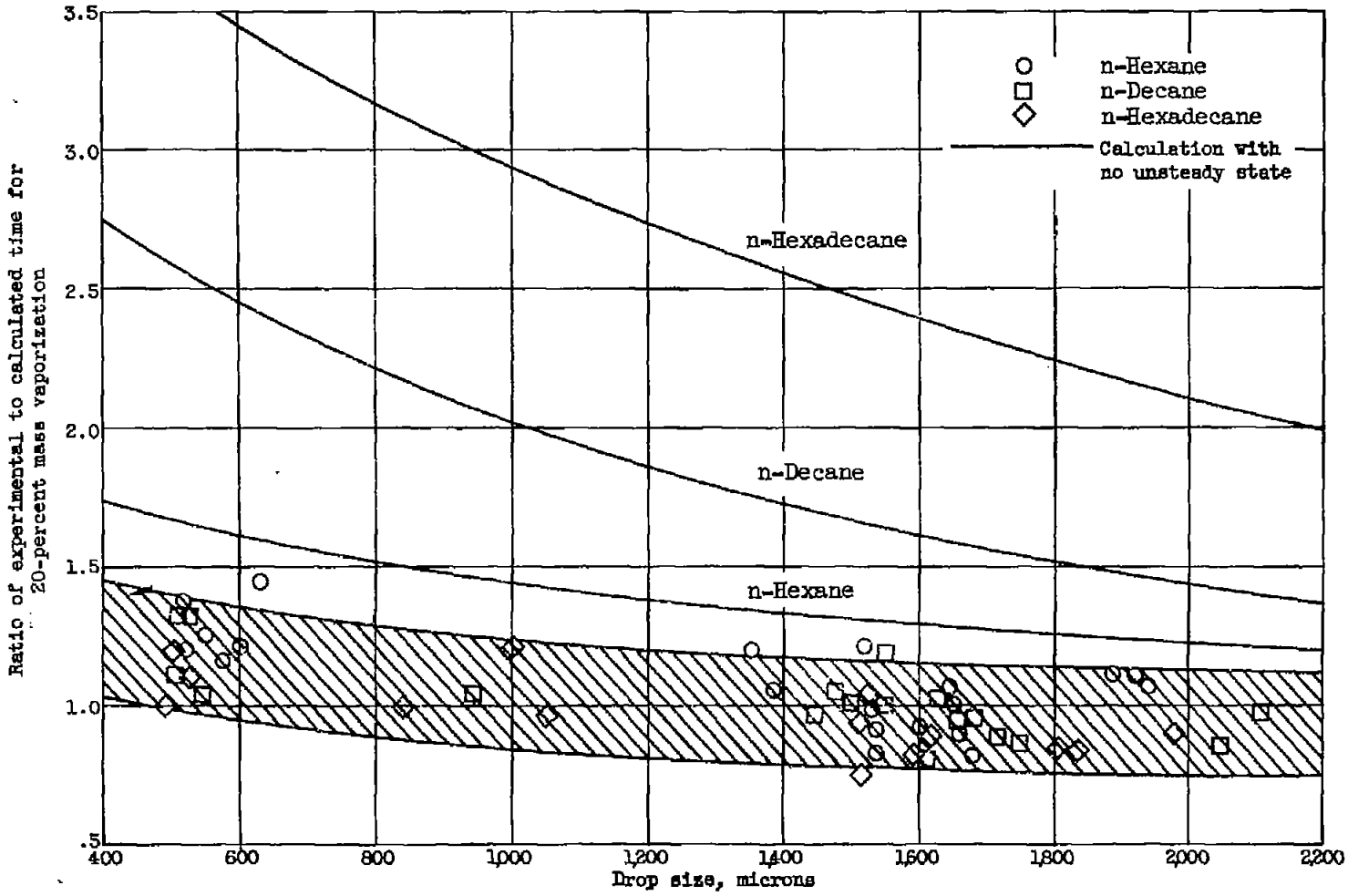

(a) Ratio for 20-percent mass vaporization.

Figure 11.- Ratio of experimental to calculated time to reach a percentage mass vaporization as a function of drop size for various fuels.

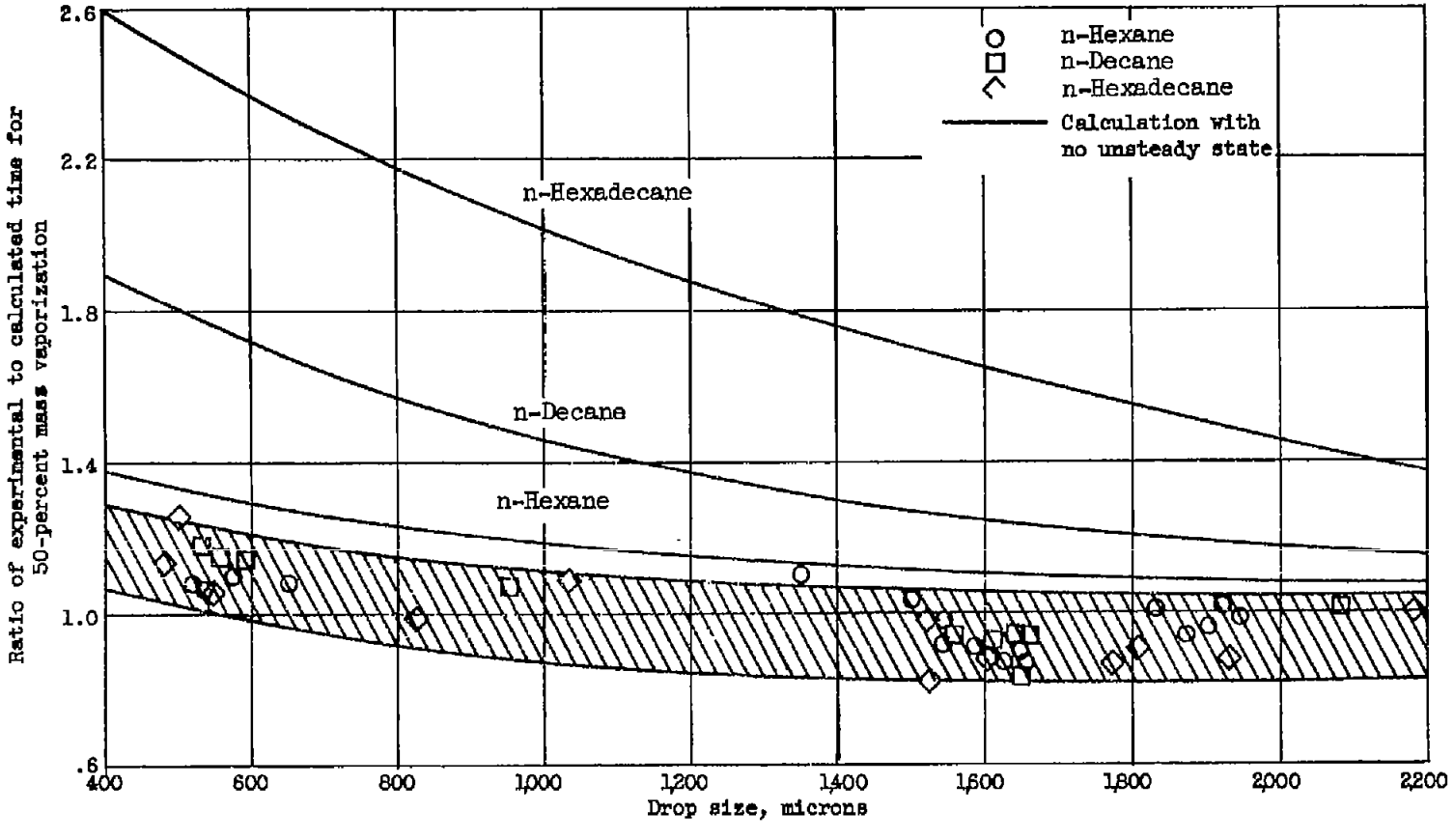

(b) Ratio for 50-percent mass vaporization.

Figure 11.- Continued.

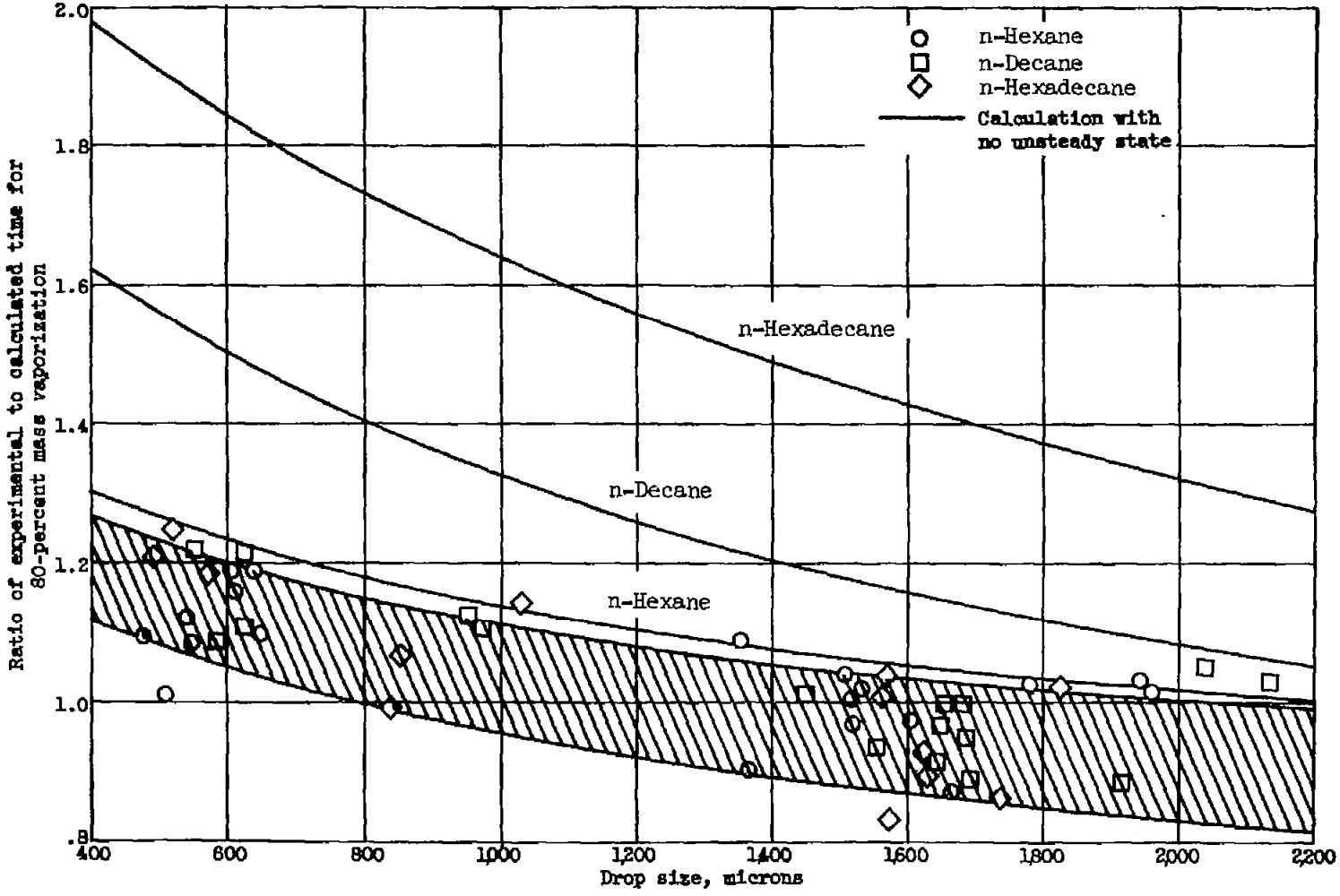

(c) Ratio for 80-percent mass vaporization.

Figure 11.- Concluded.

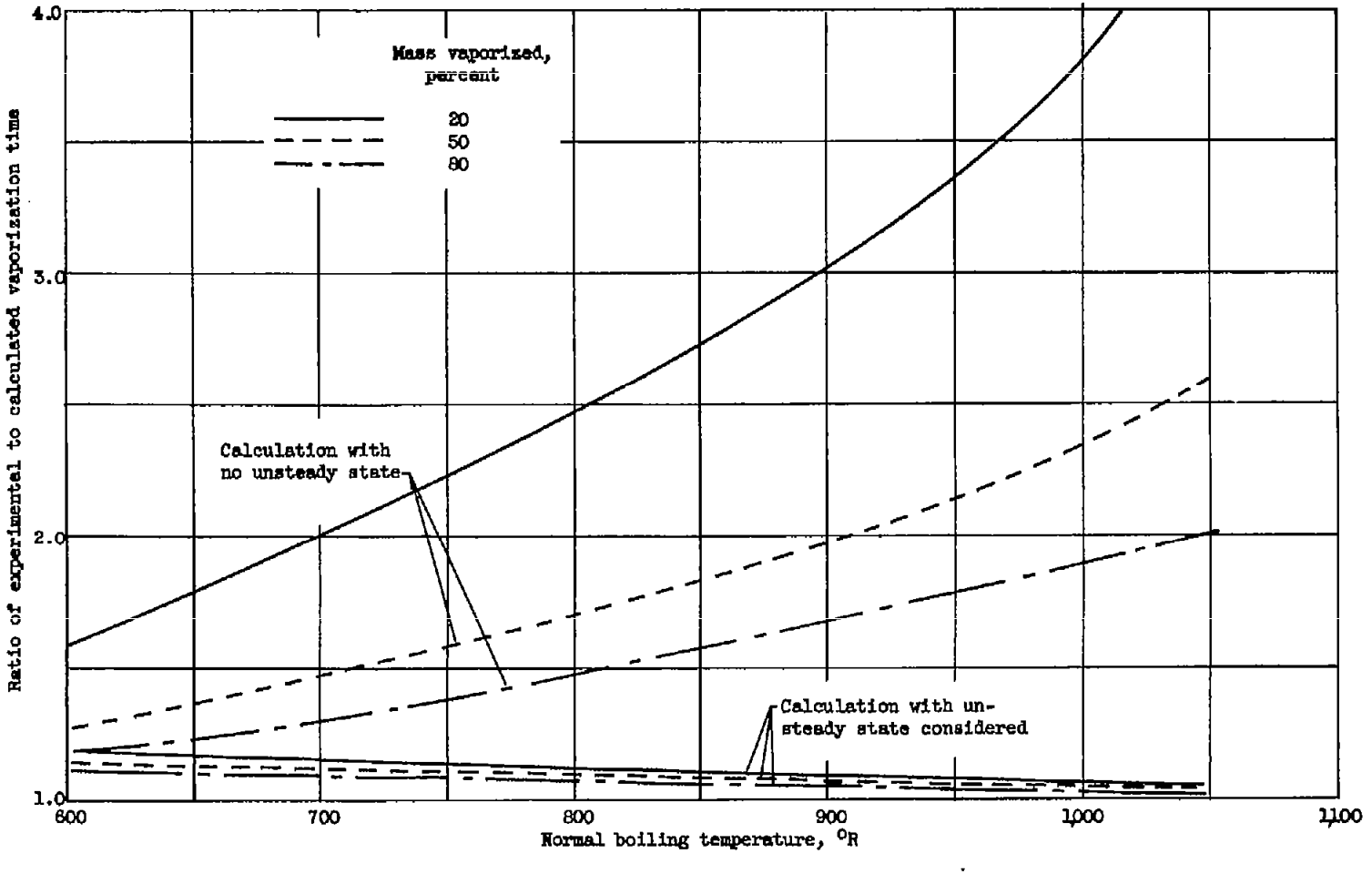

(a) Calculations with and without unsteady state considered.

Figure 12.- Comparison of ratio of experimental to calculated vaporization times with boiling temperature for various fuels. Drop size, 500 microns; air temperature, 1,300° R.

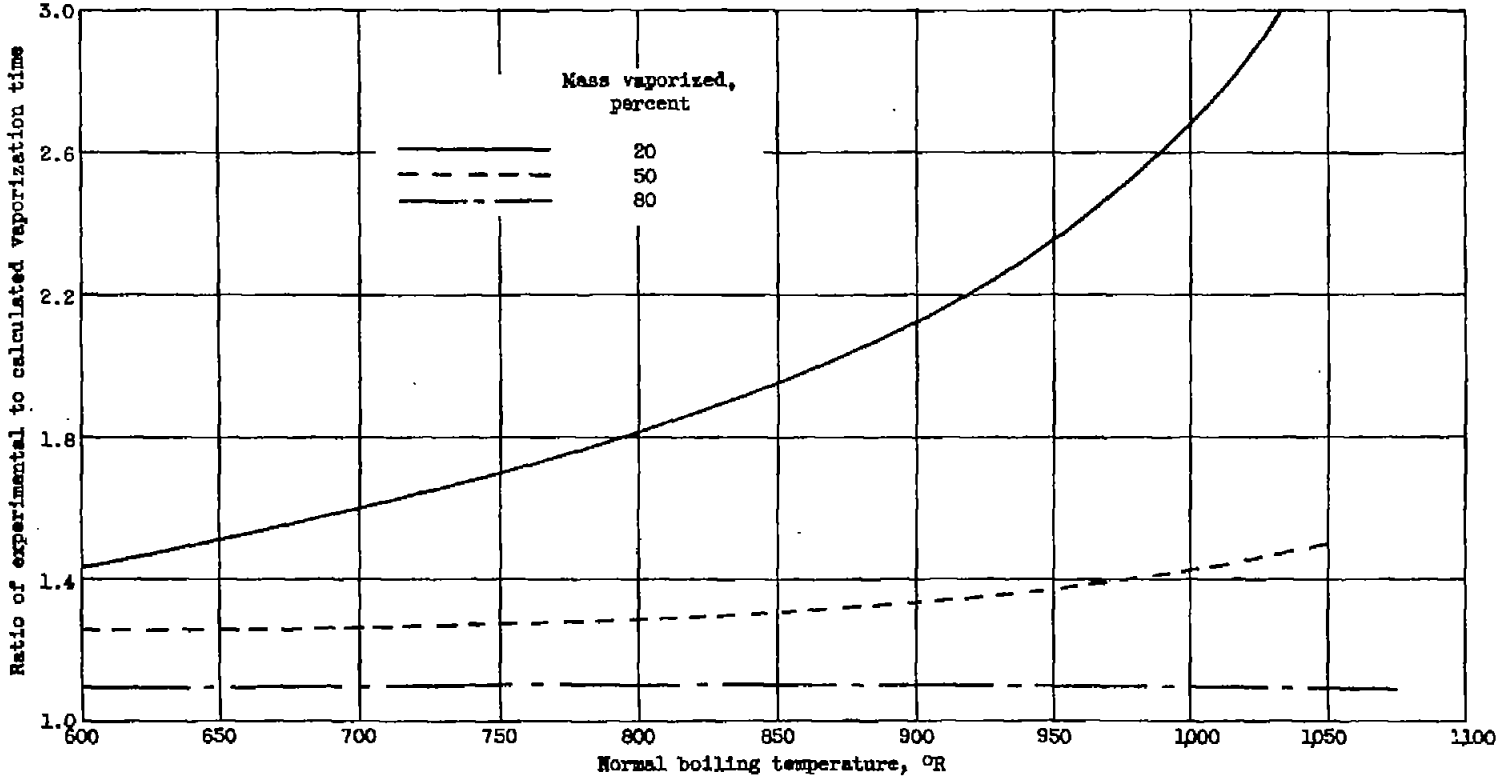

(b) Calculation performed for "zero" thermal conductivity or "peeling."

Figure 12.- Concluded.

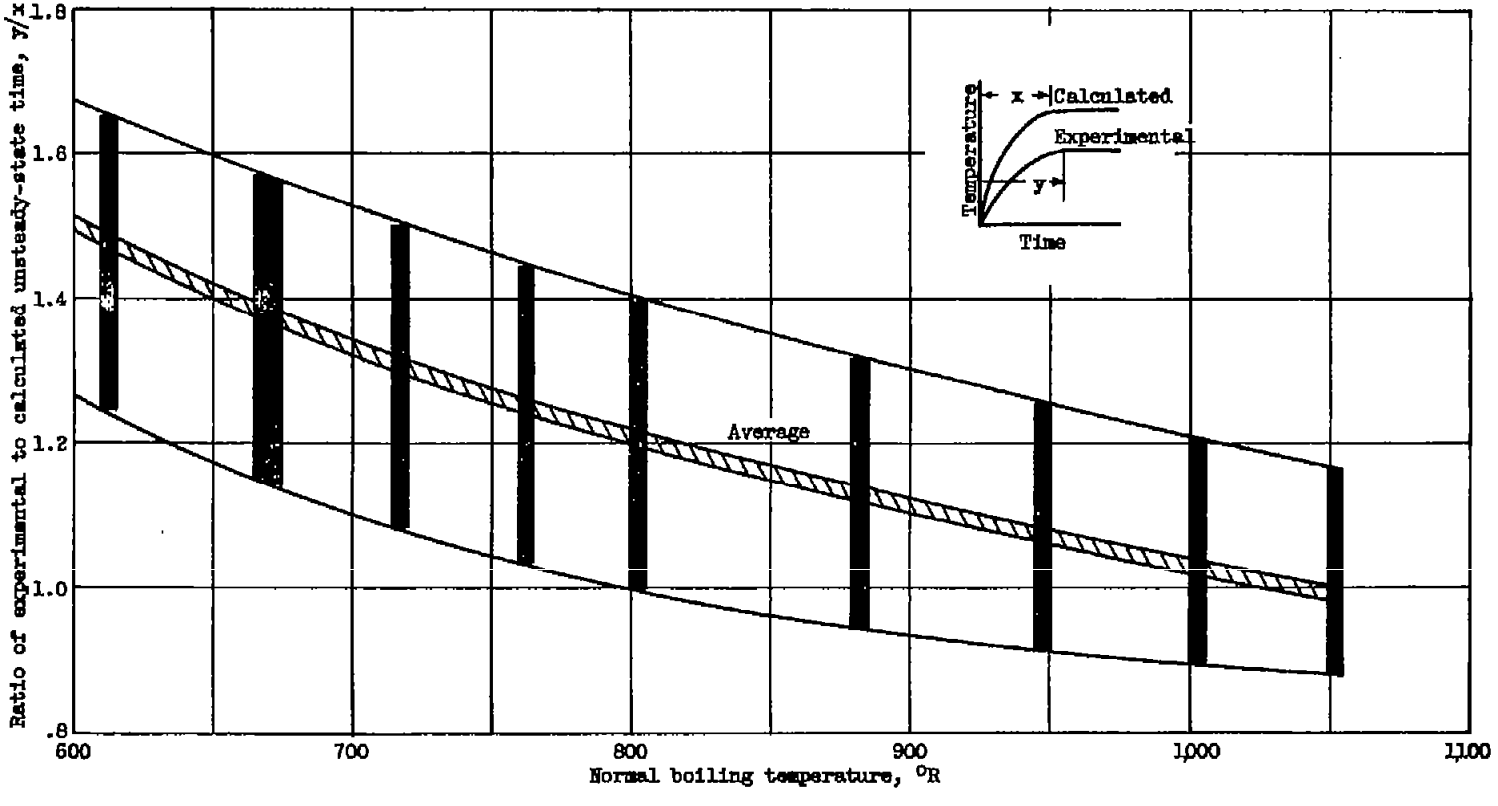

Figure 13.- Ratio of experimental to calculated unsteady-state time as a function of normal boiling temperatures for various fuels.

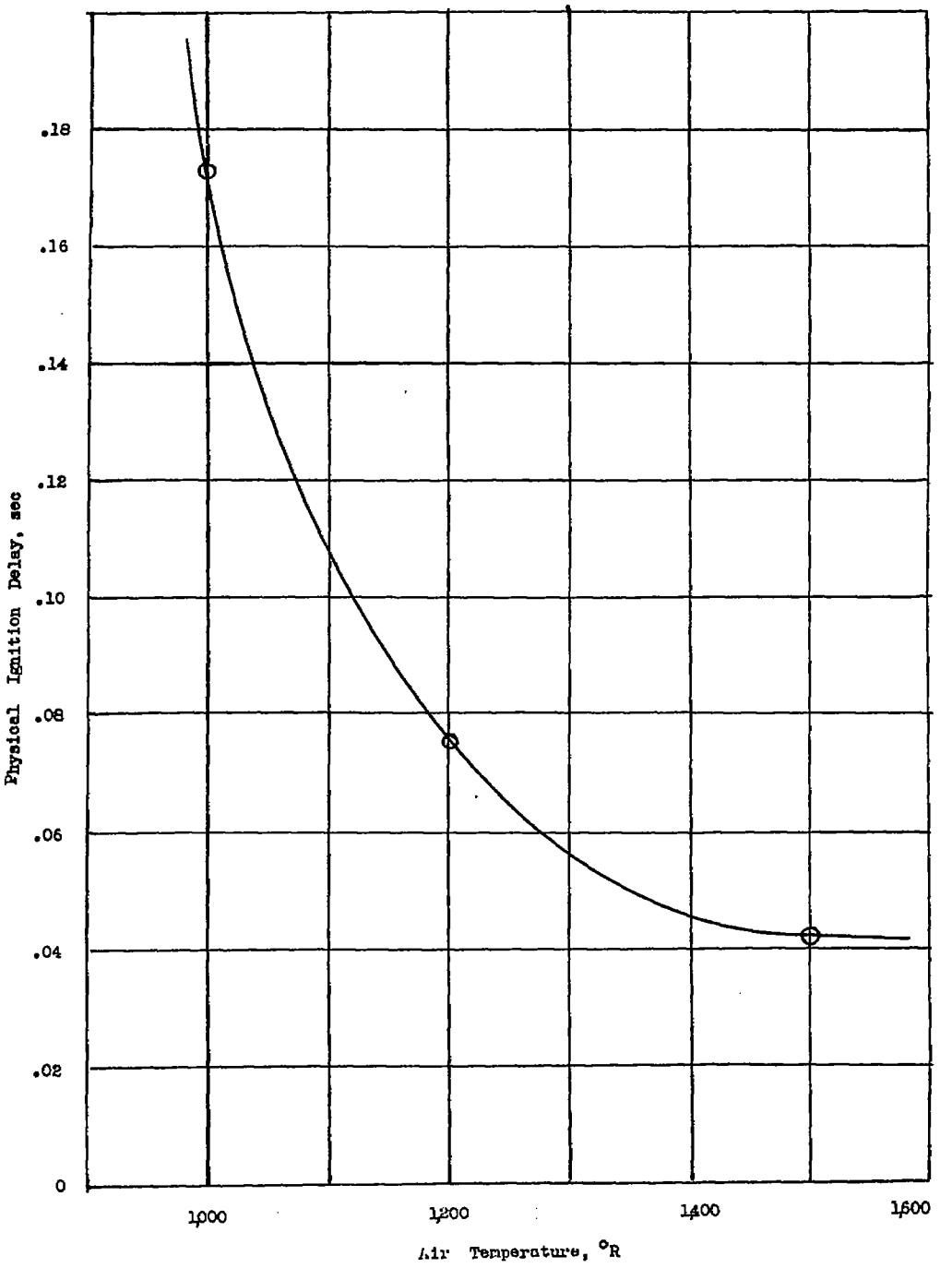

Figure 14.- Effect of air temperature on physical ignition delay of n-decane. Initial liquid temperature, 500° R; air velocity, 100 inches per second; initial drop diameter, 500 microns.

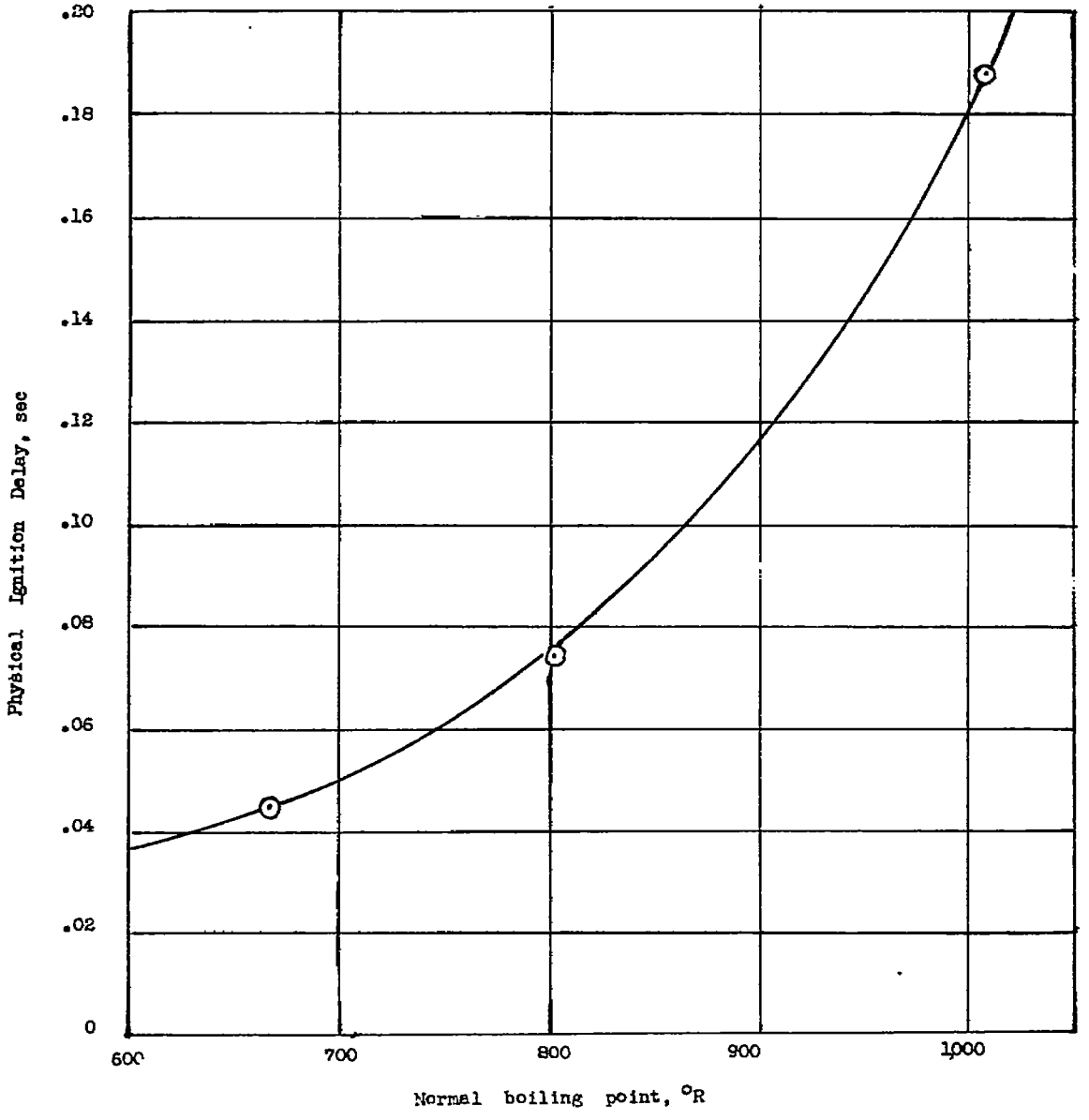

Figure 15.- Comparison of the physical ignition delay of normal paraffin fuels. Air temperature, 1200° R; air velocity, 100 inches per second; initial diameter, 500 microns; initial fuel temperature, 500° R.

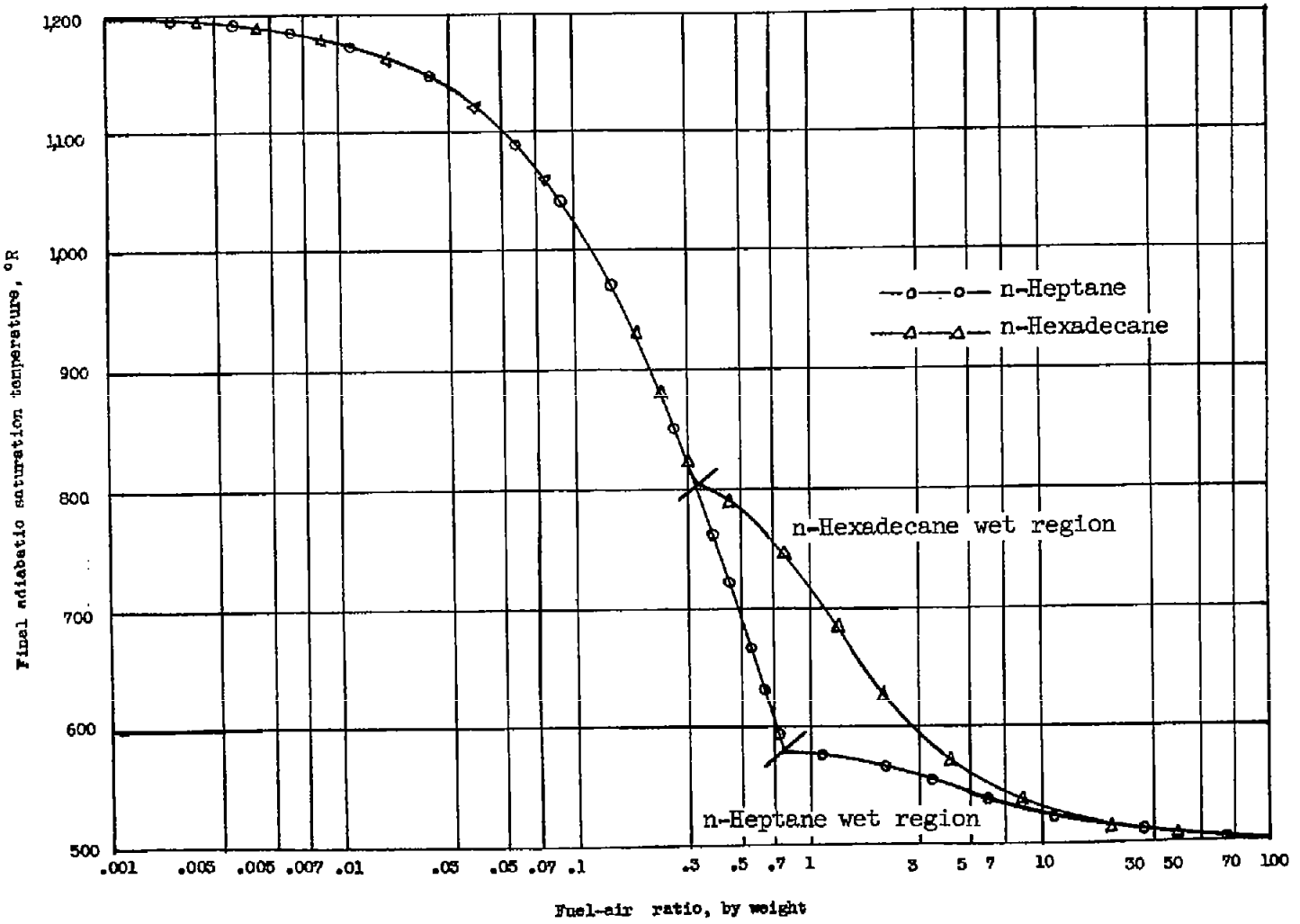

Figure 16.- Overall fuel-air ratio versus final adiabatic saturation temperature for n-heptane and n-hexadecane. Air temperature, 1,200° R; initial fuel temperature, 500° R.

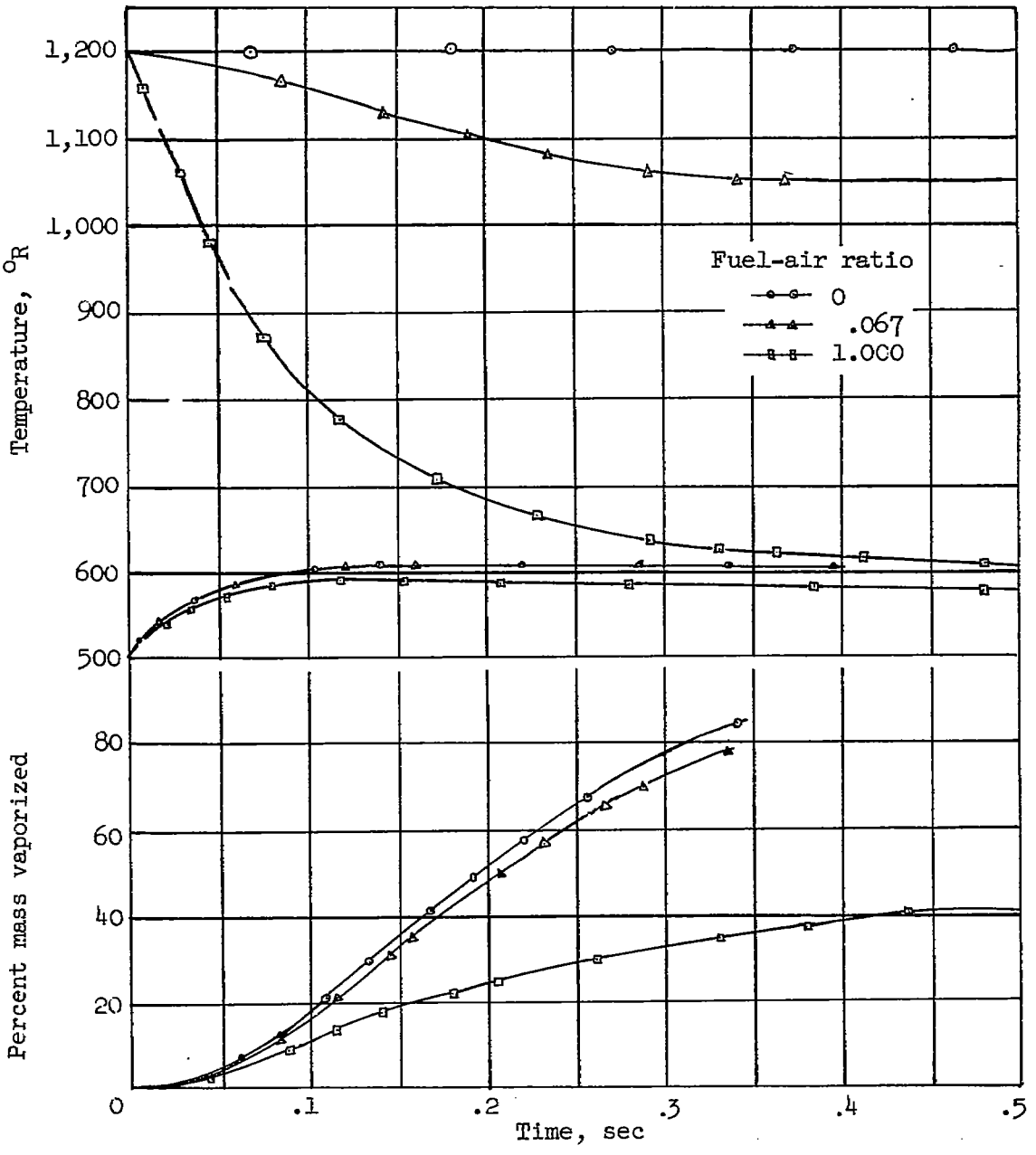

(a) n-heptane.

Figure 17.- Mass and temperature histories for various fuel-air ratios. Initial air temperature, 1,200° R; initial liquid temperature, 500° R; air velocity, 100 inches per second; initial drop diameter, 500 microns. Fuel-air ratios, 0, 0.067, and 1, as indicated.

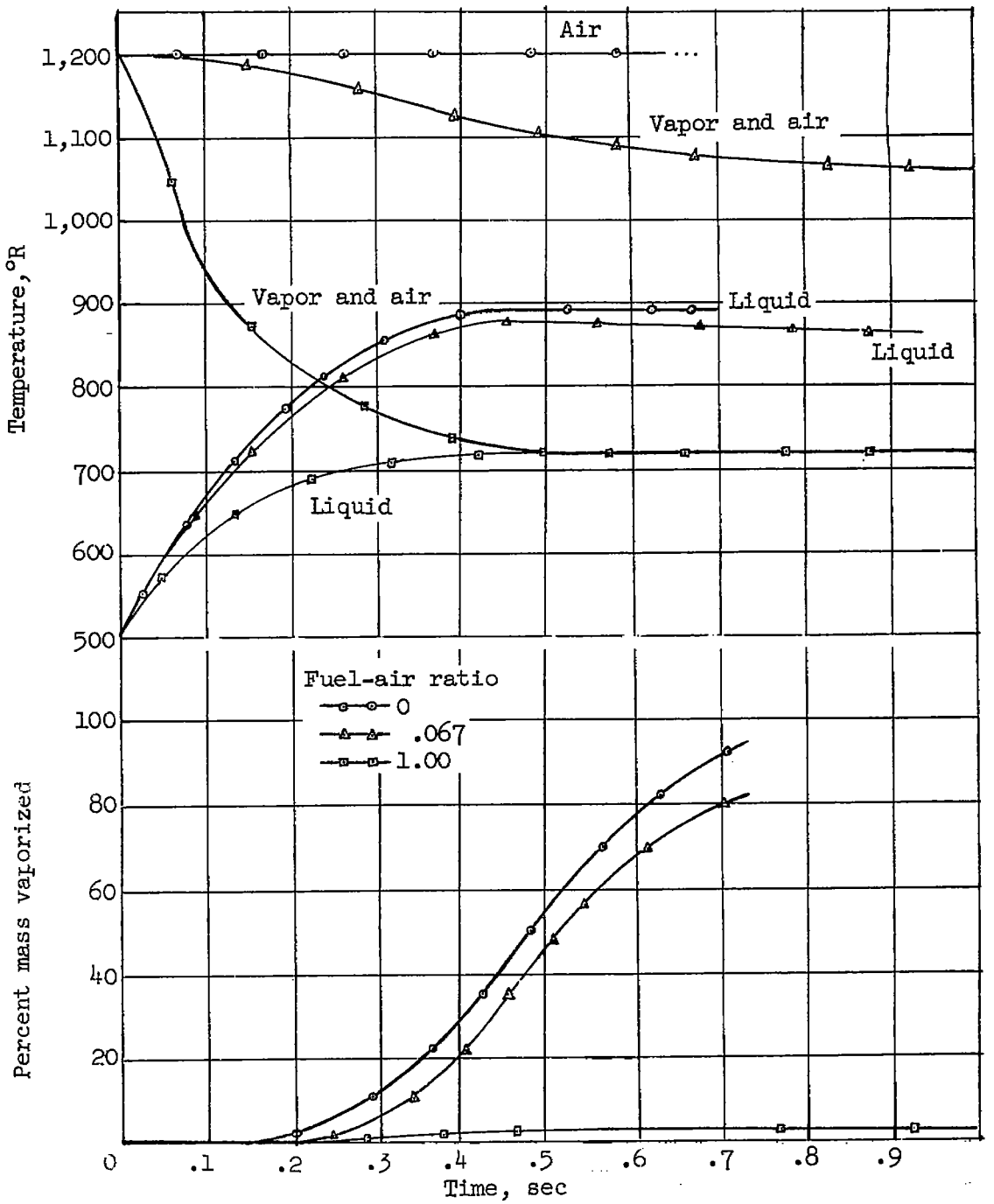

(b) n-hexadecane.

Figure 17.- Concluded.

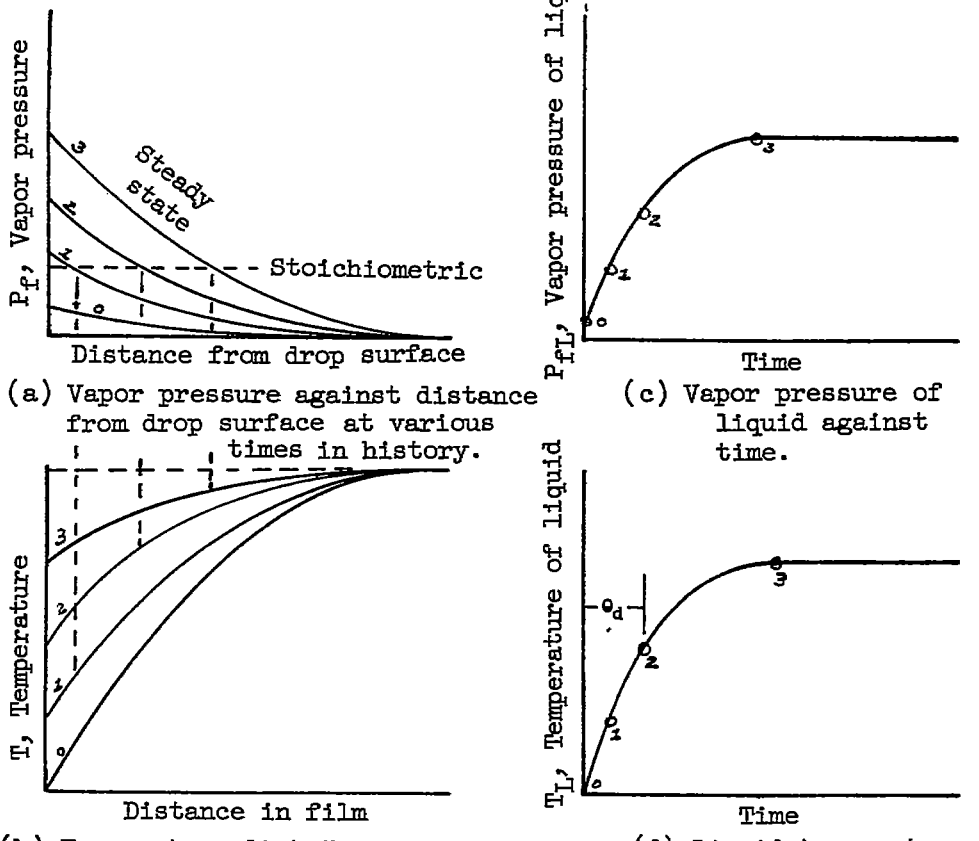

(a) Vapor pressure against distance from drop surface at various times in history.

(b) Temperature distribution in film at various times in history.

(c) Vapor pressure of liquid against time.

(d) Liquid temperature against time. θ_d, particular value of physical-ignition-delay time.

(e) Temperature of stoichiometric mixture against distance in film.

Figure 18.- Development of self-ignition mixture.

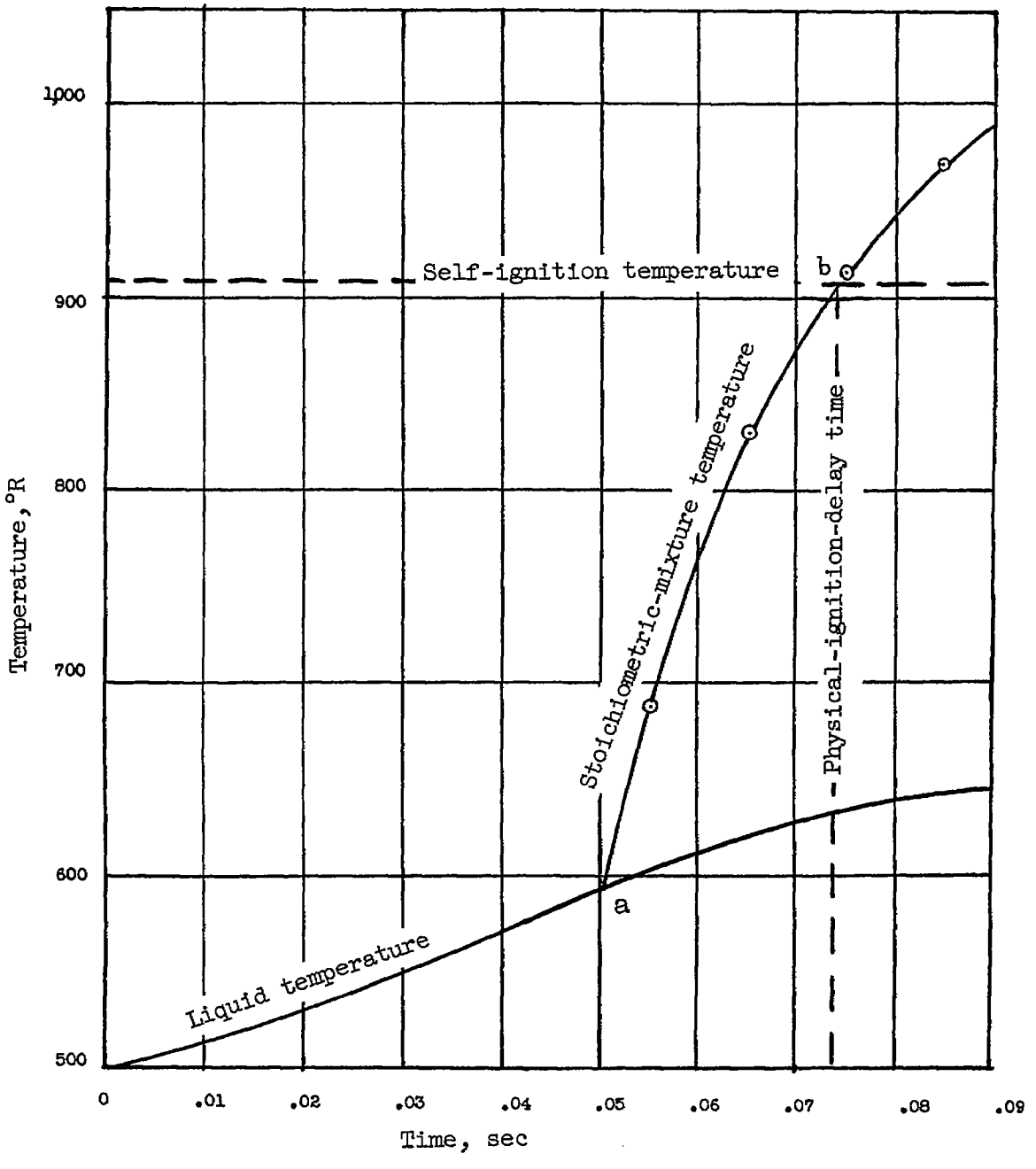

Figure 19.- Stoichometric-mixture temperature against time for n-decane; self-ignition temperature, 909° R. Air temperature, 1,200°; air velocity, 100 inches per second; initial drop radius, 500 microns.